https://doi.org/10.5194/bg-2021-339
Preprint. Discussion started: 17 December 2021

Biogeosciences
Discussions
Open Access

Downscaling CMIP6 Global Solutions to Regional Ocean Carbon Model: Connecting the Mississippi, Gulf of Mexico, and Global Ocean

Le Zhang[1] and Z. George Xue [1,2,3]

[1]Department of Oceanography and Coastal Sciences, Louisiana State University, Baton Rouge, LA 70803
[2]Center for Computation and Technology, Louisiana State University, Baton Rouge, LA 70803
[3]Coastal Studies Institute, Louisiana State University, Baton Rouge, LA 70803

Correspondence to: Z. George Xue (zxue@lsu.edu)

Abstract. Coupled physical-biogeochemical models can significantly reduce uncertainties in estimating the spatial and temporal patterns of the ocean carbon system. Challenges of applying a coupled physical-biogeochemical model in the regional ocean include the reasonable prescription of carbon model boundary conditions, lack of in situ observations, and the oversimplification of certain biogeochemical processes. In this study, we applied a coupled physical-biogeochemical model (Regional Ocean Modelling System, ROMS) to the Gulf of Mexico (GoM) and achieved an unprecedented 20-year high-resolution (5 km, 1/22°) hindcast covering the period of 2000-2019. The model's biogeochemical cycle is driven by the Coupled Model Intercomparison Project 6-Community Earth System Model 2 products (CMIP6-CESM2) and incorporates the dynamics of dissolved organic carbon (DOC) pools as well as the formation and dissolution of carbonate minerals. Model outputs include generally interested carbon system variables, such as pCO_2, pH, aragonite saturation state (Ω_{Arag}), calcite saturation state (Ω_{Calc}), CO_2 air-sea flux, carbon burial rate, etc. The model's robustness is evaluated via extensive model-data comparison against buoy, remote sensing-based Machine Learning (ML) predictions, and ship-based measurements. Model results reveal that the GoM water has been experiencing an ~ 0.0016 yr^{-1} decrease in surface pH over the past two decades, accompanied by a ~ 1.66 $\mu\mathrm{atm\ yr}^{-1}$ increase in sea surface pCO_2. The air-sea CO_2 exchange estimation confirms that the river-dominated northern GoM is a substantial carbon sink. The open water of GoM, affected mainly by the thermal effect, is a carbon source during summer and a carbon sink for the rest of the year. Sensitivity experiments are conducted to evaluate the impacts from river inputs and the global ocean via model boundaries. Our results show that the coastal ocean carbon cycle is dominated by enormous carbon inputs from the Mississippi River and nutrient-stimulated biological activities, and the carbon system condition of the open ocean is primarily driven by inputs from the Caribbean Sea via Yucatan Channel.

1 Introduction

Carbon dioxide (CO_2) concentration in the atmosphere has increased approximately 150% from 1750 to 2019 (Le Quéré et al., 2018), the storage and transport of carbon in Earth's ecosystem under the context of climate change has been receiving incremental attention over the past decades (Anav et al., 2013; Lindsay et al., 2014; Jones et al., 2016). The direction and magnitude of ocean-atmosphere CO_2 fluxes are subject to change with increasing atmospheric CO_2 concentrations (Smith &

https://doi.org/10.5194/bg-2021-339
Preprint. Discussion started: 17 December 2021

Hollibaugh 1993, Wollast & Mackenzie 1989), incremental ocean dissolved inorganic carbon (DIC) level (Torres et al., 2011), modification of the coastal alkalinity generation process (Renforth & Henderson, 2017), changes in organic matter (OM) remineralization patterns (Buesseler et al., 2020), river inputs (Yao & Hu, 2017), etc. As an enormous reservoir, the ocean has intake some 170 ± 20 PgC (Le Quéré et al., 2018) since the industrial revolution. This alleviates the CO_2 accumulation rate in the atmosphere while inducing a consequent increase in ocean carbon level and a decrease in ocean *pH* and calcium mineral saturation state (Ω, Doney et al., 2009). Given the stakes it holds in shaping climate feedback in the long term and risk for coastal ecosystems under acidification stress, carbon sink quantities and their trends have been studied and monitored by multiple works (Maher & Eyre, 2012; Czerny et al. 2013; Najjar et al., 2018; Bushinsky et al. 2019).

Nevertheless, uncertainties and mismatches in carbon flux estimates among different works and difficulties in describing the spatial and temporal pattern of pCO_2 data collected from ship-based measurements left many vital questions unanswered. Global Earth System Models (ESMs) are essential tools for studying the linkage between the ocean carbon cycle and climate change. Extensive utilization of ESMs in hindcasting and coupled biogeochemistry provide pivotal information for understanding the carbon cycle on a global scale (Anav et al., 2013; Laurent, Fennel, & Kuhn, 2021; Lindsay et al., 2014; Jones et al., 2016; Todd-Brown et al., 2014). However, their relatively coarse spatial resolution is likely not appropriate to be directly compared with field measurements. It is imperative to apply high-resolution regional ocean models to understand carbon exchange and carbon budget at a regional scale. While high-resolution regional models have been developed to represent the complex patterns of ocean circulation and elemental fluxes on the continental shelves, the regional ocean carbon system is challenging to model and predict due to its high sensitivity to the boundary and initial conditions, uncertainties in the carbon pathway, and complex interactions between the atmosphere, ocean, and land (Hofmann et al., 2011).

The Gulf of Mexico (GoM) is a semi-closed marginal sea. The presence of Mississippi-Atchafalaya River System (MARS) and the obstructions from Florida Strait and Yucatan Channel mitigate the impact from the global ocean into the GoM regarding water acidity and carbon levels. Allochthonous nutrients from river input, upwelling, and boundary shape the general pattern of the carbon cycling in the GoM (Cai et al., 2011; Chen et al., 2000; Delgado et al.,2019; Dzwonkowski et al., 2018; Laurent et al., 2017; Jiang et al., 2019; Sunda & Cai, 2012; Wang et al., 2016), and need to be properly included in the carbon system modeling in GoM. Fennel et al. (2011) performed a coupled physical-biological modeling of the northern GoM (NGoM) shelf with nitrogen cycle to describe the phytoplankton variability under the influence of the MARS covering the period of 1990-2004. They found that biomass accumulation in the light-limited plume region near the Mississippi River delta was not primarily controlled bottom-up by nutrient stimulation because of the lack of nutrient limitation in the eutrophic region. Xue et al. (2016) achieved a first GoM carbon budget and concluded that the export of carbon out of the Gulf via Loop Current is largely balanced by river inputs and influx from the air. Their regional carbon model used three sets of initial and open boundary conditions derived from empirical salinity-temperature-DIC-alkalinity relationships. Although this method of carbon system prescription leveraged the convenience of widely available physical variables and was feasible for regions with scarce

DIC and alkalinity data, its reliability was questionable as temperature and salinity alone cannot fully describe the spatial and temporal pattern of these carbon variables. Laurent et al. (2017) presented a regional model study of the eutrophication-driven acidification and simulated the recurring development of an extended acidified bottom waters in summer on the NGoM shelf. They proved that the acidified waters were confined to a thin bottom boundary layer where the production of CO_2 was dominated by benthic metabolic processes. Despite reduced Ω values being produced at bottom water due to acidification, these regions remain supersaturated with aragonite. Chen et al. (2019) presented a unified model to estimate surface pCO_2 by applying Machine Learning (ML) methods on remote sensing data and cruise pCO_2 measurements. Their ML model confirmed that the GoM was a carbon sink. Recently Gomez et al. (2020) performed another GoM carbon model study covering the period of 1981- 2014. Their model initial and boundary conditions were derived from a downscaled Coupled Model Intercomparison Project 5 (CMIP5) Modular Ocean Model (25km resolution, Liu et al., 2015). Their model results showed that GoM was a sink for atmospheric CO_2 during winter-spring, and a source during summer-fall, producing a basin-wide mean CO_2 uptake of 0.35 mol m^{-2} yr^{-1}. Nevertheless, their model does not include DOC pool or calcification process, which are imperative to describe the dynamic of DIC and alkalinity in the ocean.

Despite the above carbon system regional modeling efforts, we notice that several processes that could contribute significantly to the carbon cycle in the GoM have not been investigated yet. The carbon cycle in the ocean is linked with the nutrient cycle through photosynthetic activities, calcification, and OM remineralization (Anav et al., 2013; Farmer et al., 2021; King et al., 2015). OM remineralization could be the most critical mechanism regulating the ocean carbon system, followed by the $CaCO_3$ cycle (Lauvset et al., 2020), with the remineralization of small detritus accounting for over 40% of the DIC production on the shelf (Laurent et al., 2017). Autochthonous nutrients from direct remineralization of OM determine the gradient of DIC in the euphotic layer (Boscolo-Galazzo et al., 2021; Boyd et al., 2019). During this process, the fast-sinking of OM, higher OM particulate to dissolved ratio foster larger sedimentation rate and greater DIC removal of the euphotic layers; on the contrary, slower sinking and faster decomposition rate of OM favors nutrient and DIC retention in the euphotic layers (Davis et al., 2019; Mari et al., 2017; Turner, 2015). The remineralization of land-derived OM and $CaCO_3$ precipitation are significant factors controlling air-sea CO_2 flux (Mackenzie et al. 2004). Studies have revealed the formation of marine $CaCO_3$ (Burton and Walter,1987; Inskeep and Bloom, 1985; Zhong and Mucci, 1989; Zuddas and Mucci, 1998) and the dissolution of marine $CaCO_3$ mineral is Ω-dependent as well (Adkins et al. 2021). The Ω will be depressed with more CO_2 dissolves in seawater and can be used as an indicator for the buffering capacity of the ocean carbonate system. Given that Ω influences the calcification rate of marine organisms and regulates the acidity of bottom waters, it should be considered in the $CaCO_3$ cycle for a comprehensive carbon cycle assessment.

In this study, we dynamically downscaled the solution of the latest Coupled Model Intercomparison Project 6 (CMIP6) product to a regional model to inherit the climate perturbation signals (Liao et al., 2020) and the accumulative effect of carbon variables from the global solutions. Our regional model includes critical carbon cycle processes lacking in previous efforts, including the most up-to-date carbonate chemistry thermodynamic parameterization, phosphate cycling, formation & dissolution of $CaCO_3$, and the inclusion of the DOC as a semi-labile carbon pool. The objective of this study is 1) to assess the feasibility and robustness of utilizing downscaled global model products to drive a regional coupled physical-biogeochemical model, and 2) to examine the temporal trend of key variables of the carbon system (pCO_2, pH, air-sea CO_2 exchange, and Ω) of the surface ocean in the GoM. In addition, to evaluate the impact of MARS and the global ocean on GoM's carbon cycling, two perturbed experiments are designed. The following sections are organized: model setup is given in Sect. 2; in Sect. 3, we validate the model's performance against buoy, remote sensing-based ML solution, and ship-based measurements; the trend of key carbon systems over the past two decades are given in Sect. 4; an assessment of the contribution of riverine inputs and global ocean are discussed in Sect. 5, together with a model uncertainty analysis.

2 Method

2.2 Model setup

Our model is built on the platform of Coupled Ocean-Atmosphere-Wave-Sediment Transport modeling system (COAWST; Warner et al., 2010). COAWST is an open-source community model which includes the Model Coupling Toolkit to allow data exchange among three state-of-the-art numerical models: Regional Ocean Modelling System [ROMS, svn 820, Haidvogel et al., 2008; Shchepetkin and McWilliams, 2005], the Weather Research and Forecasting model [WRF, Skamarock, et al., 2005], and the Simulating Waves Nearshore model [SWAN, Booij et al., 1999]. The carbon model presented in this study is based on a well-validated coupled physical-biogeochemical model by Zang et al. (2019 and 2020), which covers the entire GoM waters (Gulf-COAWST, Fig. 1). The Gulf-COAWST has a horizontal grid resolution of ~5 km and 36 sigma-coordinate (terrain-following) vertical levels. A third-order upstream horizontal advection and fourth-order centred vertical advection are used for momentum and tracer advection. The biogeochemical model is developed based mainly on the pelagic N-based biogeochemical model Pacific Ecosystem Model for Understanding Regional Oceanography (NEMURO, Kishi, et al., 2007; Kishi et al., 2011). In this study, we extend the number of the NEMURO's state variables from seven to seventeen, including nitrate (NO_3), ammonium (NH_4), two phytoplankton groups (small phytoplankton, diatom), one explicit phosphorus pool PO_4, two pools of silicon (particulate silica, and silicic acid), three zooplankton groups (micro-zooplankton, meso-zooplankton, and predator-zooplankton) and two pools of detritus containing carbon (particulate organic nitrogen [PON], particulate inorganic carbon [CalC], a dissolved organic carbon (DOC) pool, a dissolved organic nitrogen pool (DON), oxygen (O_2) to regulate the availability of aerobic OM remineralization, dissolved inorganic carbon (DIC) for bookkeeping the sum of dissolved inorganic carbon species in water, and total alkalinity (TA) for bookkeeping the acid neutralization capacity of water. The stoichiometry between carbon and nitrogen in the OM production and remineralization is set to 6.625 following Fennel (2008).

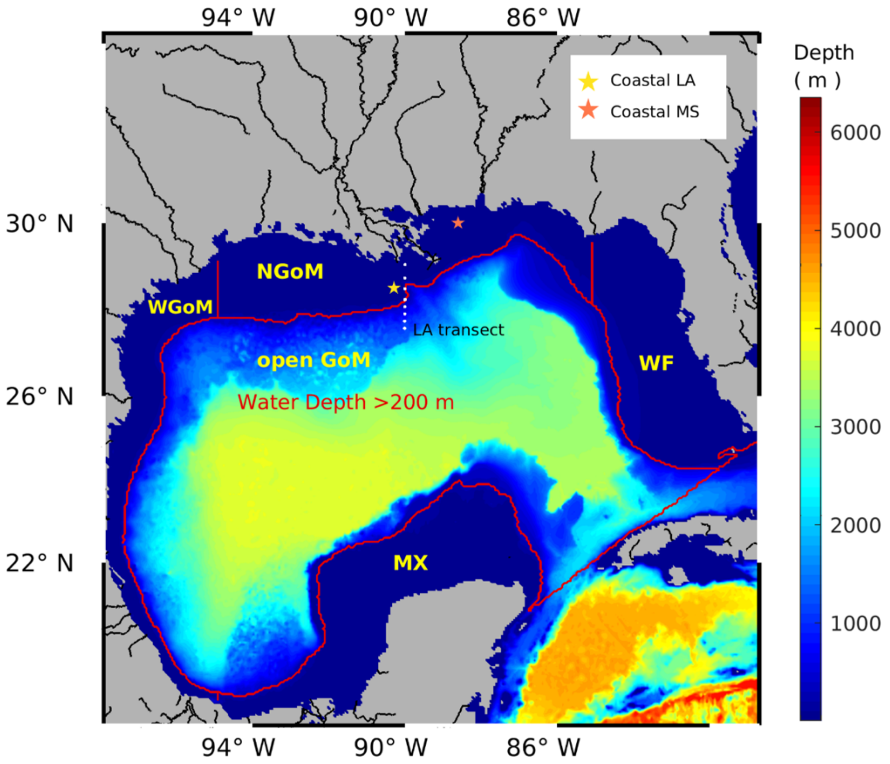

Figure 1: Gulf-COAWST model domain with water depth in color (unit: m). Subregional definitions followed Xue et al. (2016), which are Mexico Shelf (MX), Western Gulf of Mexico Shelf (WGoM), Northern Gulf of Mexico Shelf (NGoM), West Florida Shelf (WF), and Open GoM.

The revised biogeochemical model incorporates key processes regulating the carbon model, including primary production, river DIC, PON and DOC delivery, sediment carbon burial, CO_2 air-sea flux, $CaCO_3$ cycling, and OM remineralization (Fig. 2). Widely used carbon system variables, such as pCO_2, pH, Ω, etc., are used as carbon system state indicators. The carbon module that takes in DIC, TA, PO_4, Si (dissolved inorganic silicon), salt, temp, for calculating pCO_2, pH, Ω_{Arag}, and Ω_{Calc}, largely followed the recommended best practices (Dickson, Sabine, & Christian, 2007; Eyring et al., 2016; Orr et al., 2017; Zeebe and wolf-Gladrow, 2001), with an updated parameter prescription for dissociation constants for carbonic acid ($K1$) and bicarbonate ion ($K2$) (Millero, 2010), and solubility products for aragonite K_A and calcite K_C (Mucci, 1983).

Inorganic carbonate mineral (mainly $CaCO_3$) forms during the photosynthetic activities of some phytoplankton species and foster aggregation of detritus and their sinking. The rate of $CaCO_3$ production followed a dynamic ratio regarding primary production of small phytoplankton with low-temperature inhibition and enhancement during bloom conditions (Moore et al., 2004). The production and dissolution of $CaCO_3$ are important processes for ocean acidity regulation, as its production (by 1 unit) nominally takes away a unit of [CO_3^{2-}] from water, which reduces the alkalinity and DIC by 2 and 1 unit, respectively. This process routinely happens during photosynthetic activities of some phytoplankton species (such as coccolithophores, parameterized implicitly as a portion of small phytoplankton in this model) and other marine calcifiers. Carbonate minerals produced in the euphotic zone could be treated as equivalent storage of alkalinity and are usually transported towards the ocean sediment through sinking. Aragonite and calcite are two common mineral phases of $CaCO_3$ secreted by marine organisms and are included in the model. Ω_{Calc} and Ω_{Arag} are calculated as the equilibrium product of Ca^{2+} and $CO_3{}^{2-}$. When $\Omega > 1$, calcification is thermodynamically favored, and when $\Omega < 1$, dissolution is thermodynamically favored. As defined in Eq. (1), [Ca^{2+}] and [CO_3^{2-}] are the concentrations of calcium and carbonate ions, respectively. [Ca^{2+}] is determined through salinity (Millero, 1982; Millero, 1995), and [CO_3^{2-}] is calculated through the model carbon module. K_{sp} is the stoichiometric solubility product mainly dependent on pressure, temperature, and salinity. K_{sp} is defined for aragonite and calcite as K_A and calcite K_C, respectively.

$$\Omega = \frac{[Ca^{2+}][CO_3^{2-}]}{K_{sp}} \quad (1)$$

In our model, the sediment pool of sinking particles is a simplified representation of burial and benthic remineralization processes, where the flux of sinking materials out of the bottommost grid point is added to the sediment pool and entered the burial pool (remain inactive) with a dynamic ratio, the active sediment pools undergo enzyme-aided decomposition at rates regulated by temperature and oxygen, and release corresponding influx of ammonium, DIC, and alkalinity at the sediment/water interface. Our model uses a CO_2 production ratio of 0.138 between sediment aerobic respiration and denitrification (Fennel et al., 2006) and an alkalinity production ratio of 1.93 between pyrite burial and denitrification (Hu & Cai, 2011). Upon being sunk to acidified regions, the dissolution of $CaCO_3$, regulated by Ω, can consume dissolved CO_2 and neutralize the acid.

The bulk formula for air-sea gas exchange for CO_2 is used following Wanninkhof (1992). Air-sea CO_2 flux is calculated as Eq. (2).

$$F_{CO2} = k_{660} \left(\frac{Sc}{660}\right)^{-1/2} s\, \Delta pCO_2 \quad (2)$$

Where F_{CO2} is the air-sea CO_2 flux in the unit of mmol CO_2 m^{-2} d^{-1}. *Sc* is the Schmidt number (nondimensional) (calculated following Wanninkhof, 2014), *s* is the solubility of CO_2 in seawater in mol CO_2 m^{-3} μatm^{-1} (calculated following Weiss, 1974), and Δ pCO_2 is the air and sea pCO_2 difference in µatm. The term k_{660} is the quadratic gas transfer coefficient in cm h^{-1} (converted to m d^{-1}). We calculated the air-sea CO_2 flux using the relationships of gas exchange with wind speed at 10 m over the sea surface (U_{10}) following Wanninkhof (1992). We used the ocean convention for the CO_2 flux, i.e., a positive flux is defined as the ocean being a sink of atmospheric CO_2. Air pCO_2 level is prescribed using fitted curve from column-averaged dry-air mole fraction of atmospheric carbon dioxide from 2002 to present derived from satellite product (merged dataset from SCIAMACHY/ENVISAT, TANSO-FTS/GOSAT, and OCO-2 [https://cds.climate.copernicus.eu/; Dils et al., 2014]).

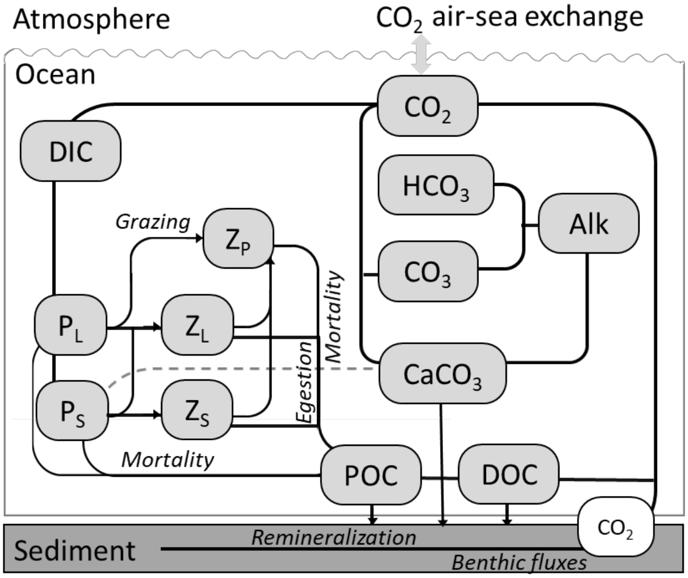

Figure 2: Schematic showing major processes incorporated in the carbon cycle.

We performed a 20-yr model hindcast covering the period of 1 January 2000 – 31 December 2019. The model setup was similar to that of Zang et al. (2020), with ocean physical initial and boundary conditions downscaled from the 1/12° data assimilated Hybrid Coordinate Ocean Model (HYCOM/NCODA, GLBu0.08/expt_19.1, expt_90.9, expt_91.0, expt_91.1, expt_91.2, and expt_93.0 [https://www.hycom.org; Chassignet et al. 2003]). Atmospheric forcings include ground level or sea surface downwelling shortwave/longwave radiation, ground-level or sea surface upwelling shortwave/longwave radiation, surface air pressure, surface air temperature, relative humidity, precipitation, wind at 10 m were extracted from the NCEP Climate Forecast System Reanalysis (CFSR) (Saha et al. 2010) and Climate Forecast System Version 2 (CFSv2) (Saha et al. 2011). Boundary conditions of the biogeochemical variables (DIC, DOC, TA, NO_3, PO_4, Si, NH_3 are extracted from The Intergovernmental Panel on Climate Change (IPCC) CMIP6 global solution (CESM2-WACCM-FV2, historical, r1i1p1f1, nominal resolution 100 km, [Danabasoglu, 2019]). Due to the global model ending in December 2014, the biogeochemical boundary condition of 2014 was used repeatedly for the period of 2015-2019. O_2 is absent from the CESM2-WACCM-FV2 source, and is interpolated from the World Ocean Atlas 2018 (WOA18) product (Boyer et al, 2018; García et al., 2019). Freshwater and terrestrial nutrient inputs from 47 major rivers discharged to the GoM are applied as point sources. River discharge and water quality data of rivers in the U.S. are collected from US Geological Survey (USGS) stations (https://maps.waterdata.usgs.gov), river DOC is prescribed following the values reported by Shen et al. (2012), with additional reference from several other works (Reiman & Xu, 2019; Stackpoole et al., 2017; Wang et al., 2013; Xu & DelDuco, 2017). Mexican river discharge data are collected from BANDAS (https://www.gob.mx/conagua), water quality data of Mexican rivers is prescribed as the average of that of the Mississippi and Atchafalaya rivers. River nutrient and carbon load are reconstructed from available USGS observations. Missing river alkalinity values are interpolated from climatological values, and missing river DIC values are calculated from *pH* and alkalinity using the MATLAB program CO2SYS (Lewis & Wallace, 1998). Validations of the model's performance in physics, nutrient cycle, and primary production can be found in Zang et al., 2019 and 2020. In this study, we focus on the model's performance in the carbon cycle, which is presented in the next section.

The simulation is set to start on 2000-01-01 and end in 2019-12-31. Since model simulated DIC concentration in the water column is sensitive to initial conditions (Hofmann et al., 2011; Xue et al., 2016), using initial condition from a snapshot (January 2000) of the global model result would be appropriate as the global model has been well stabilized up to the year 2000 from its "pre-industry" experiment. Nevertheless, we treated the first year of the simulation (2000) as the model spin-up, and all results presented below are based on model outputs from 2001 to 2019 unless otherwise specified. To quantify the impact from river discharge and global ocean on the carbon system in the GoM, in addition to the control experiment where the historical product of the CESM2-WACCM-FV2 experiment is applied as the boundary conditions (from here, experiment "His"), two perturbed experiments, "Bry" and "NoR" are added. The Bry experiment has a clamped DIC and TA conditions as that of the year 2000 for all following years while keeping all other experiment setups the same as that of the His. The NoR experiment eliminates the presence of all rivers in the model while keeping the rest of the experiment set up the same as that of the His. As by far most available observations are confined in the surface ocean, except for the GOMECC transects, in this study, we focus on the surface ocean carbon condition in the NGoM and Open GoM waters.

3 Validation

This section focus on the validation of the model results via comparison against autonomous mooring systems with surface pCO_2 measurements, ship-based measurements from the Gulf of Mexico Ecosystems and Carbon Cruise transects (GOMECC, Barbero et al., 2019; Wanninkhof et al., 2013; Wanninkhof et al., 2016), and pCO_2 underway measurements (data downloaded from https://www.ncei.noaa.gov/access/oads/). Direct observations of the GoM carbon system have been recognized as unbalanced among seasons due to fewer data points available in winter compared to other seasons. To overcome the sporadic direct measurement dataset, we also performed a model-data comparison against the remote sensing-based ML product of sea surface pCO_2 by Chen et al. (2019).

3.1 Model–buoy comparisons

Temporal variability of sea surface pCO_2 was recorded by the autonomous mooring system at two sites (CoastalMS and coastal LA) operated by the Atlantic Oceanographic and Meteorological Laboratory (AOML) of the National Oceanic and Atmospheric Administration (NOAA). The CoastalMS buoy site (location see Fig. 1, data coverage: 2009-01-14 to 2009-12-09; 2011-03-17 to 2012-08-04; 2013-07-10 to 2014-02-10; 2014-02-10 to 2014-05-03; 2014-12-12 to 2015-03-22; 2015-03-30 to 2016-09-22 2016-09-23 to 2017-05-29) is predominately impacted by the Mississippi River followed by the coastal ocean, whereas the CoastalLA buoy site (data coverage: 2017-07-14 to 2017-11-07; 2017-12-14 to 2019-04-26; 2019-06-04 to 2020-08-12; 2020-08-12 to 2021-08-25; 2021-08-25 to 2021-11-29) is mutually influenced by the Mississippi River and the coastal ocean. The high-frequency measurements provide a time-resolved picture of year-round changing pCO_2 values. Temperature and salinity can influence the chemical equilibrium in the carbonate system, therefore shifting the pCO_2 values. Validating the temperature and salinity at these two mooring sites is a prerequisite before looking into the surface pCO_2 levels. In Fig. 3, the top four panels compare the sea surface temperature (SST) and salinity (SSS) between model and buoy measurements and show matching seasonal variability. At CoastalMS, the range for sea surface pCO_2 is 150~600 µatm. Sea surface pCO_2 records are more volatile at CoastalLA with a maximum value > 800 µatm and a minimum value around 150 µatm. Following the salinity drop, pCO_2 at the CoastalMS site is simultaneously reduced, demonstrating the river's influence on both salinity and pCO_2. At CoastalLA, however, the pCO_2 level does not necessarily follow the trend of salinity, implying complex controlling factors in addition to the river inputs. The bottom two panels of Fig. 3 show a good agreement between measured and simulated sea surface pCO_2. We notice model-data discrepancies in April 2018-04 at CoastalLA and July 2011 at CoastalMS and ascribe such bias to the uncertainty in the riverine DIC inputs prescription and the limited model horizontal resolution (~5 km).

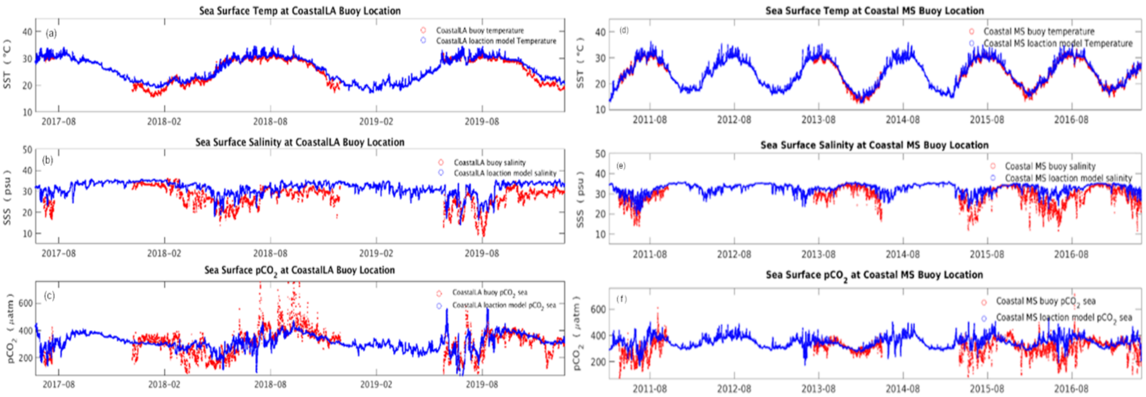

Figure 3: Timeseries of SST, SSS, and pCO_2_sea at site CoastalLA and CoastalMS.

3.2 Model–cruise comparisons

Cruise carbon measurements include underway water pCO_2 data and conductivity–temperature–depth (CTD) bottle results. We compare the model result at the LA transect with the observations of GOMECC cruises, conducted at the same location during GOMECC1 in 2007, GOMECC2 in 2012, and GOMECC in 2017, respectively. Measurements of TA during GOMECC cruises followed Dickson's definition (1981), where the TA is expressed as Eq. (3)

$$TA = [HCO_3{}^-] + 2[CO_3{}^{2-}] + [B(OH)_4{}^-] + [OH^-] + [HPO_4{}^{2-}] + 2[PO_4{}^{3-}] + \\ [H_3SiO_4{}^-] + [NH_3] + [HS^-] - [H^+] - [HSO_4{}^-] - [HF] - [H_3PO_4] - [HNO_2] \qquad (3)$$

Equation (3) contains fourteen variables, among which $[PO_4{}^{3-}]$ are explicitly modeled as active tracers, $[HCO_3{}^{-}]$, $[CO_3{}^{2-}]$, $[B(OH)_4{}^{-}]$, $[OH^{-}]$, $[HPO_4{}^{2-}]$, $[H_3SiO_4{}^{-}]$, $[H^{+}]$, $[HF]$, $[H_3PO_4]$ are calculated by the carbon module, and $[HS^{-}]$, $[HSO_4{}^{-}]$, $[HNO_2]$, $[NH_3]$ are unaccounted. Figure 4 shows the vertical profiles of observed DIC, TA, and their ratio collected at the LA transects (-90°W, 27.5°N - 29.1°N, shown in Fig.1) overlaid with the model solution. All three transects were taken during August when nutrient supply from the MARS was high. Model simulated profiles at the transects match well with the in situ CTD data. Relative low surface DIC concentration (< 2150 mmol m^{-3}) above 200 m isobath demonstrates the river's influence in NGoM. The general increasing trend of DIC with depth confirms the presence of a biological pump, where inorganic carbon is utilized during photosynthesis in the euphotic layer. Subsequently, the generated OM sinks into deeper waters while being remineralized along the way. The TA profiles show more variation compared with DIC, where generally a lower TA concentration (< 2380 millequivalent m^{-3}) could be found at the surface as the direct dilution from river discharge, follow by a quick increase to ~2380 millequivalent m^{-3} in the euphotic layer due to the active photosynthetic activities, which generate alkalinity. Further deep, the TA profiles show a decreasing trend between 200 and 700 m, which could be explained by the water column respiration and nitrification. The TA profiles show a slow increase from 800 m and deeper, which coincides with the alkalinity generation processes in sediment and possibly dissolution of carbonate minerals, both adding to the bottom water TA. The TA/DIC ratio has a maximum at the surface due to low DIC concentration and decreases with depth as DIC concentration increased.

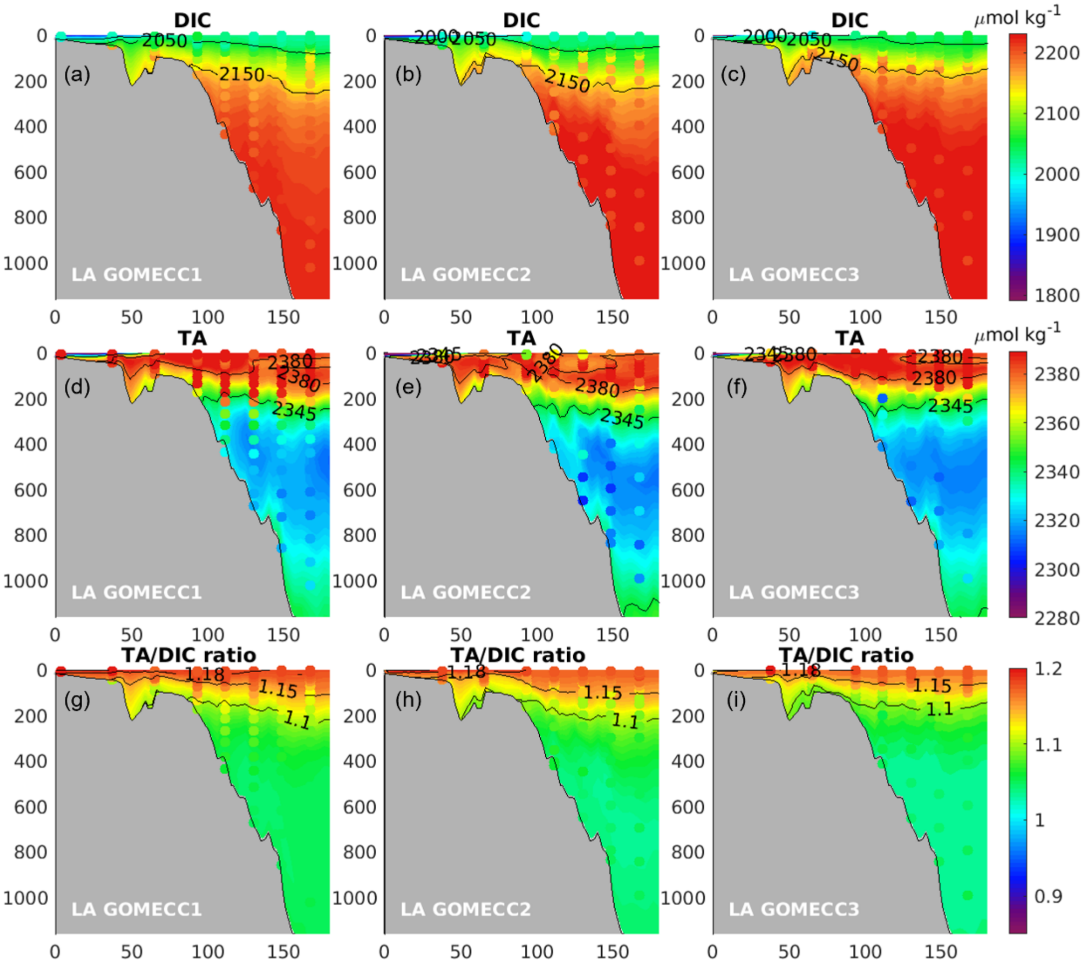

Figure 4: Discrete measurement of DIC, TA along the LA transect during GOMECC1, GOMECC2, and GOMECC3 cruises shown as scattered dots, compared with model results in color contour, with the water depth shown on the left side of each figure in meter.

3.3 Model–ML *pCO*$_2$ product comparisons

Direct comparison between cruise measurement of ocean surface *pCO*$_2$ and daily averaged model result might suffer from systematic bias due to the sparsity of curies data, both temporally and spatially. The ML model generates surface *pCO*$_2$ from Chen et al. (2019) integrated >220 cruise surveys between 2002-2019 and MODIS ocean color product covering 2002-2017. Comparison between the two surface *pCO*$_2$ products are shown in Fig. 5, where surface *pCO*$_2$ results from Chen et al. (2019) are denoted as "ML" and results from this work are denoted as "Model" for the monthly climatology from July 2002 to December 2017. The two results exhibit a highly similar spatial distribution of surface *pCO*$_2$, with our model result demonstrating substantial influence from the Loop Current. Compared with the ML model, our model produces lower pCO_2 estimates over NGoM during winter and fall, higher pCO_2 estimates over WF during summer, and stronger influence from the Caribbean Sea. Chen et al. (2019) reported that no satellite data was found for pCO_2 <145 µatm or >550 µatm during their 285 model development. This can also be a factor when considering the differences between the two products.

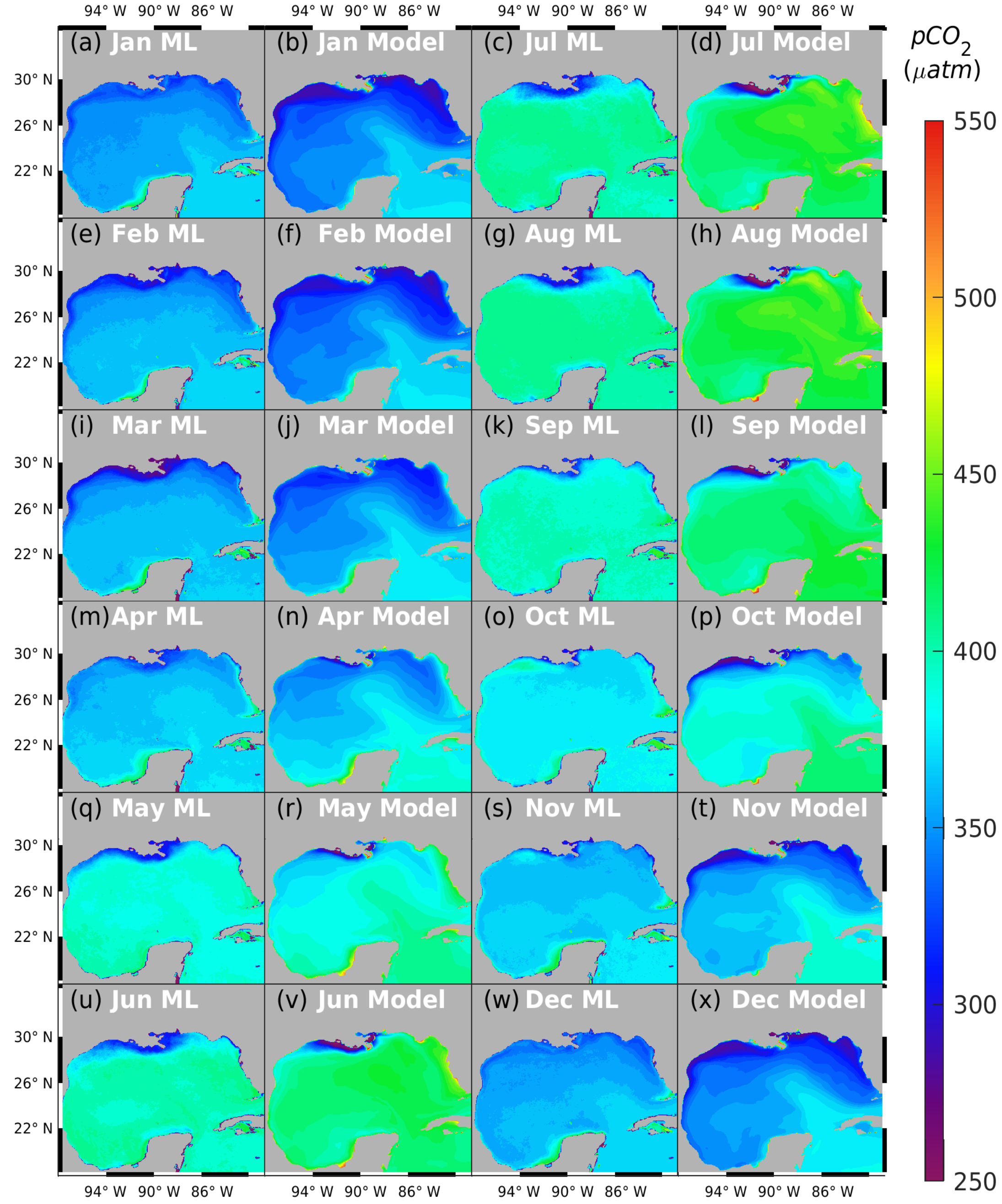

Figure 5: Comparison of surface pCO_2 between ML model (Chen et al, 2019) and this work.

https://doi.org/10.5194/bg-2021-339
Preprint. Discussion started: 17 December 2021

Besides buoy records, transects, and the ML products, we also perform an extensive model-data comparison using available ship-based underway pCO_2 measurements from the Ocean Carbon and Acidification Dataset (https://www.ncei.noaa.gov/access/oads/). Our model can capture both spatial and temporal variability in the underway pCO_2 dataset as well (Fig. S1 and Fig. S2). These extensive model-data comparisons give us the confidence that our model, driven by carbon boundary conditions from the global model, can reproduce temporal, spatial, and vertical variability of the CO_2 dynamics in the GoM.

4 Result

In this section, we present the spatial and temporal pattern of key carbon system variables, namely pCO_2, pH, Ω, and air-sea CO_2 flux simulated over the past 20 years in the GoM. In this study, we emphasize the surface carbon condition in two regions: NGoM and Open GoM, where most existing in situ data are distributed. We perform a linear fit of the time series of the key carbon system variables in each region and show the fitted relationships in Fig. 6. The slopes of the fitted linear plot give estimations on the change rate of each carbon variable over the past two decades.

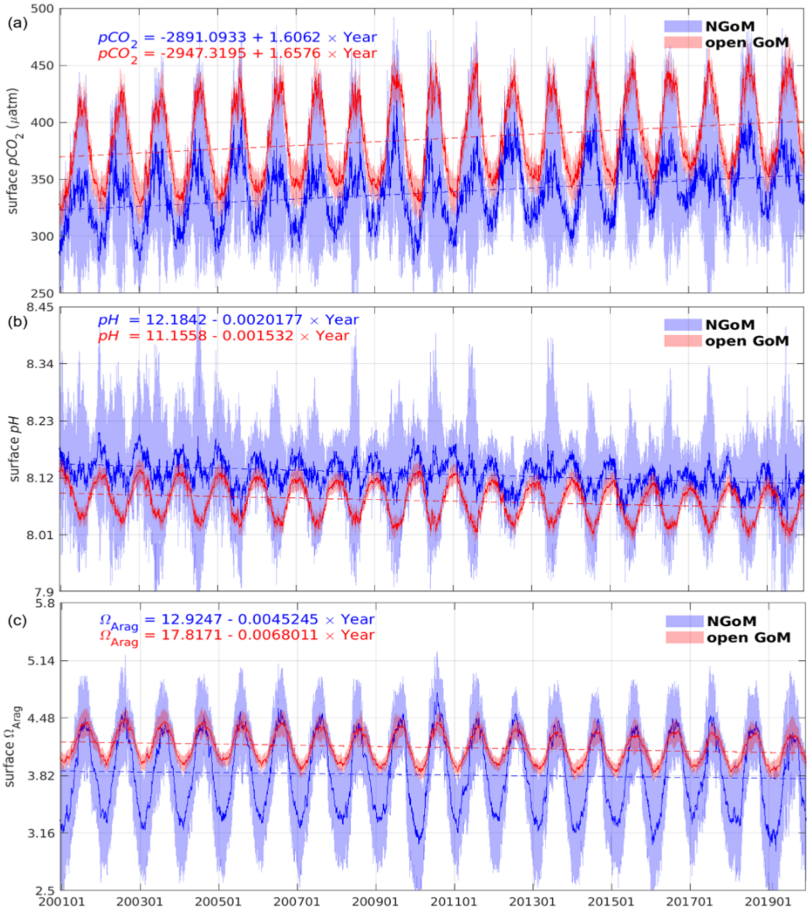

Figure 6: Time series and trend analysis of sea surface (a) *pCO_2*, (b) *pH*, (c) *Ω_{Arag}* for NGoM (blue), Open GoM (red). Solid lines depict the daily spatial mean value; shaded areas stand for 1σ standard deviation, dash lines trace the linear fit of the time series.

4.1 pCO_2

We simulate a generally increasing trend in surface pCO_2 level for both NGoM and Open GoM, with an increasing rate of 1.61 µatm yr^{-1} and 1.66 µatm yr^{-1}, respectively (Fig. 6). Seasonal ocean surface pCO_2 variation is primarily affected by temperature variations. To evaluate the pCO_2 trend without temperature effects, we decouple the thermal and nonthermal components of pCO_2 at the ocean surface using Eq. (4) and (5) and further extract the pCO_2 variation due to gross primary production and air-sea CO_2 flux. The temperature sensitivity of CO_2, γ_T = 4.23% per degree Celsius, proposed by Takahashi et al. (1993), is used to perform the thermal decoupling by multiplying the mean pCO_2 value with SST induced difference described in Eq. (4). The nonthermal counterpart is obtained by removing the thermal effect from the pCO_2 time series using Eq. (5). pCO_2 variations due to gross primary production are estimated from the carbon module based on the DIC consumed by gross primary production and denoted as pCO_2^{GPP}. pCO_2 variations due to air-sea CO_2 flux are calculated from the carbon module based on the DIC change from the air-sea exchange and denoted as pCO_2^{flux}.

$$pCO_2{}^{th} = < pCO_2 > \ exp(\gamma_T \cdot (SST - < SST >)) \quad (4)$$

$$pCO_2{}^{nt} = pCO_2 \cdot exp(\gamma_T \cdot (< SST > - SST)) \quad (5)$$

Figure 7 shows the seasonal and spatial patterns of four decoupled pCO_2 components, namely the $pCO_2{}^{th}$, $pCO_2{}^{nt}$, $pCO_2{}^{GPP}$, and $pCO_2{}^{\mathrm{flux}}$. The $pCO_2{}^{th}$ patterns in the top row (a)(b)(c)(d) of Fig. 7 reflect the fluctuation of pCO_2 due to thermal effects. Over the four seasons, a general pattern of rising $pCO_2{}^{th}$ from spring to summer and a gradual reduction from summer onwards can be observed. The NGoM shelf exhibits the lowest $pCO_2{}^{th}$ values during winter, while WF shows elevated $pCO_2{}^{th}$ values during summer. The higher $pCO_2{}^{th}$ values dwelling in the southern part of the Yucatan shelf reveal the warm water flowing into the GoM from the Caribbean Sea. The second row (e)(f)(g)(h) of Fig. 7 shows the nonthermal component of pCO_2. The relatively high $pCO_2{}^{nt}$ during winter on the NGoM shelf, compared to that of the Open GoM, shows the strong solvation effect of CO_2 with low SST, contributing to a high DIC/TA ratio and strong carbon uptake. The lower two rows of Fig. 7 show pCO_2 changes due to the gross primary production and CO_2 air-sea exchange, respectively. The $pCO_2{}^{GPP}$ reflects the intensity of primary production in terms of pCO_2 reduction. $pCO_2{}^{GPP}$ has larger magnitudes in NGoM during spring and summer and is gradually attenuated during and after fall. The large magnitudes of $pCO_2{}^{GPP}$ during summer in NGoM waters and Open GoM region following the extension of MARS plume, suggesting strong biological CO_2 removal in those regions. These results show that gross primary production has a stronger regulation on surface pCO_2 during spring and summer in river-dominated waters and upwelling regions. While a minor contribution from gross primary production can be seen during winter, on the flat and shallow WF, and in Open GoM regions southern of Loop Current. The $pCO_2{}^{\mathrm{flux}}$ reflects the intensity of air-sea CO_2 exchange attempting to mitigate the air-sea disequilibrium caused by local physical and biological processes. The relatively high value of $pCO_2{}^{nt}$ and low magnitude of $pCO_2{}^{GPP}$, as well as low river discharge (minimal river water mixing) in the WF during winter, indicate a strong CO_2 uptake from the atmosphere due to low SST. This analysis agrees with the low $pCO_2{}^{th}$ and the high $pCO_2{}^{\mathrm{flux}}$ values in the WF during winter shown in Fig. 7(d)(p). Situations during seasons other than winter are more complicated due to active biological activities and mixing. The Mississippi delta region has a high $pCO_2{}^{th}$ value during summer, however, combined with effects of mixing and strong primary production (large magnitude of $pCO_2{}^{GPP}$), this region acts as a strong carbon sink that exhibits a high value of $pCO_2{}^{\mathrm{flux}}$ compensated from the atmosphere. Figure 7 demonstrates that most of the time around the year, the surface pCO_2 pattern is not dominated by a single factor but a synthesis of multiple controlling processes. The result of pCO_2 decomposition agrees with the current view of the pCO_2 dynamic and carbon uptake patterns in the GoM, which is strong carbon uptake during winter due to thermal effect and high biological CO_2 drawdown during spring and summer under the riverine influence.

https://doi.org/10.5194/bg-2021-339
Preprint. Discussion started: 17 December 2021

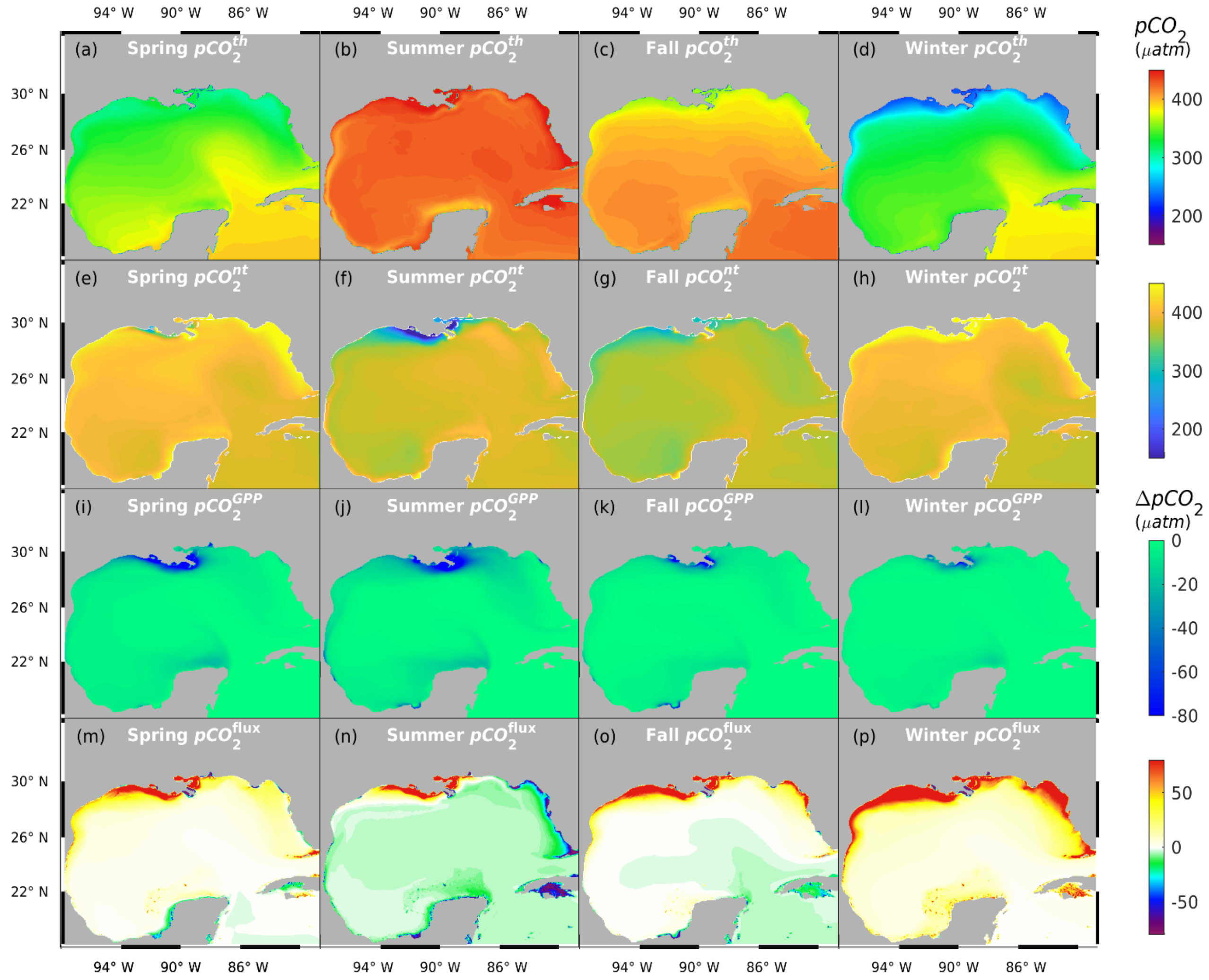

Figure 7: Spatial distribution of sea surface pCO_2 over four seasons. From the top row to bottom row: pCO_2^{th}, pCO_2^{nt}, pCO_2^{GPP}, pCO_2^{flux}

4.2 *pH*

Ocean surface *pH* in the GoM shows a clear decreasing trend, with a 0.0020 yr^{-1} decrease over the NGoM region and a 0.0015 yr^{-1} decrease over the Open GoM region. Figure 8 shows the seasonal pattern of ocean surface *pH* over the GoM. Spatial and seasonal *pH* patterns show larger variation over the NGoM, especially on the inner shelf (depth<50m). The *pH* level in the surface water is closely associated with temperature, photosynthetic activities, and water mixing. The high *pH* value on the NGoM shelf reveals the strong influence of riverine alkalinity export and nutrient-stimulated primary production. The lower *pH* values on the WF shelf during summer and the generalized greater *pH* values over NGoM during winter demonstrate the high *pH* sensitivity on SST. The upwelling region along the west Yucatan shelf shows reduced *pH* values all year round compared with its surrounding waters. The upwelling along the WGoM slope has a similar effect of reducing and maintaining a relatively low *pH*, effectively forming a *pH* boundary between the shelf water and the Open GoM. The Open GoM is largely dominated by the warmer and lower *pH* water from the Caribbean Sea throughout the year.

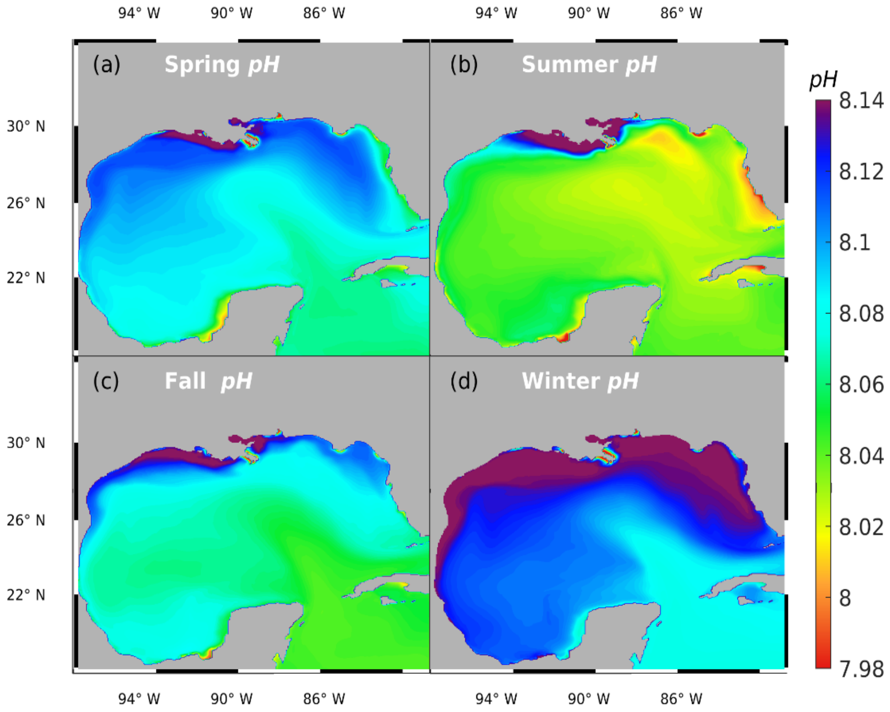

Figure 8: Seasonal averaged sea surface *pH* over 2001-2019

4.3 Aragonite and Calcite Saturation State

Aragonite undersaturation occurs ($[CO_3^{2-}] < 66$ µmol kg^{-1}) before calcite undersaturation ($[CO_3^{2-}] < 42$ µmol kg^{-1}) (Feely, Doney, & Cooley, 2009; Feely et al, 2002), as a result, Ω_{Calc} is approximately 50% higher than Ω_{Arag} and their spatial and seasonal variations are very similar as shown in Fig. 9. Variations in temperature, alkalinity, and pCO_2 impose important controls on Ω_{Arag}. The multiyear variability of Ω_{Arag} at the ocean surface is shown in Fig. 6(c). The NGoM region shows a smaller decreasing trend in Ω_{Arag} (0.0045 yr^{-1}) compared to that of Open GoM (0.0068 yr^{-1}). Noted the data contained in Fig. 6 does not include water from the shallow shelf waters (water depth < 10 m), therefore the trend in NGoM does not incorporate the condition in coastal estuaries. The spatial distribution of Ω_{Arag} across the GoM depicts a healthy level of Ω and a low risk of ocean acidification (Fig. 9). While the coastal ocean generally has a relatively high Ω level, some coastal locations warrant special attention when evaluating their tendency towards calcium mineral dissolution. These locations include coastal regions that experience a large load of riverine OM inputs (e.g., the Mississippi River delta in summer) and the upwelling regions that receive relatively higher acidity water from the bottom ocean (e.g., west of Yucatan). These regions show significant Ω reductions compared to the surrounding waters and are the potential primary victim of ocean acidification. The influence from the river on Ω is complex, on one hand, a high nutrient level of river discharge could stimulate a high photosynthetic rate which consumes DIC and increases Ω, on the other hand, photosynthesis favors calcification which consumes carbonate ion and reduces Ω. Therefore, Ω is subject to increase with stronger photosynthesis and decrease with stronger calcification. Therefore the magnitude of the overall effect will depend upon photosynthetic rates and the calcification rate. In this work, two phytoplankton groups are modeled, diatom (silicifying), and small phytoplankton (implicitly include the calcifying coccolithophores, foraminifera, and dinoflagellates), of which only the small phytoplankton group has the potential to conduct calcification (Raven & Giordano, 2009). Besides being regulated by temperature and small phytoplankton concentration, the calcification rate also depends on the composition of the phytoplankton population. The small phytoplankton group has a survival advantage at relatively low nitrogen concentrations and could be grazed by two zooplankton groups (meso-zooplankton and micro-zooplankton), whereas diatom is more nutrient-demanding and can be grazed by three zooplankton groups (predator zooplankton, meso-zooplankton, and micro-zooplankton). The competitive phytoplankton evolution shaped the relative rates between photosynthesis and calcification on the NGoM shelf during summer. The reduced Ω to the east of the Mississippi River delta is a combined result from high DIC water entrained by Loop Current eddies west of the delta, and an increased ratio of small phytoplankton in offshore waters.

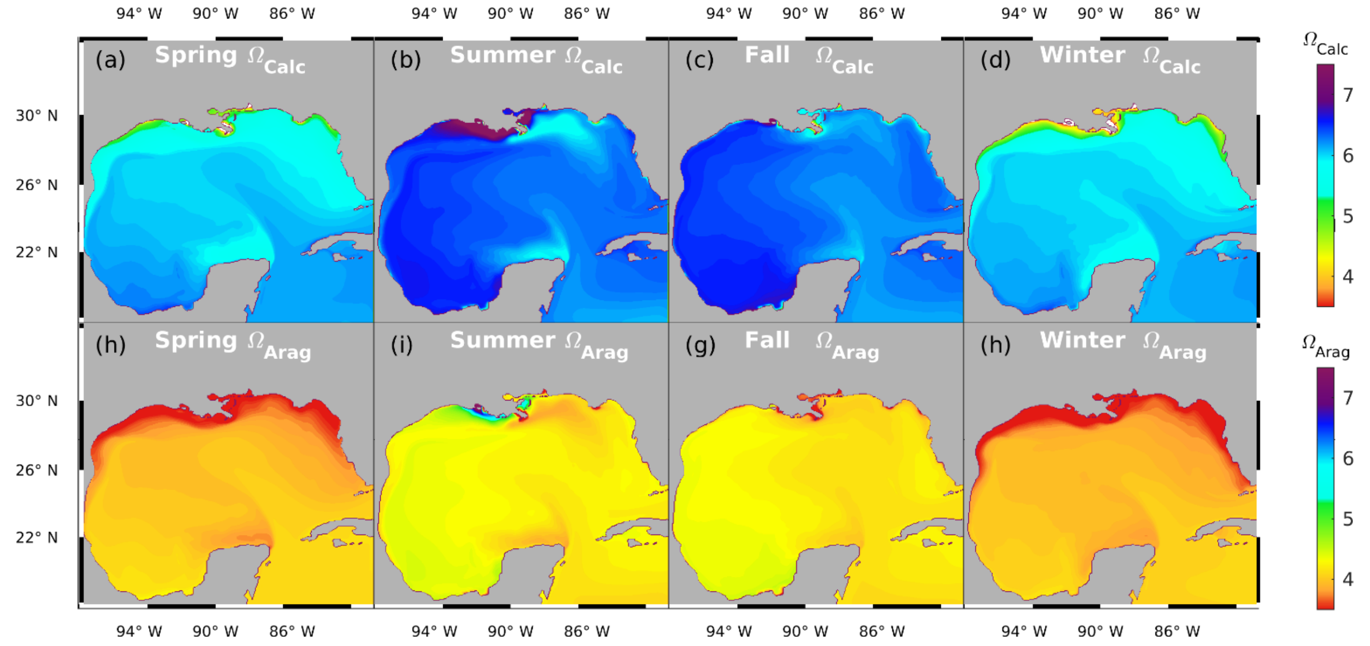

Figure 9: Seasonal mean sea surface Ω_{Arag} and Ω_{Calc} over 2001-2019

4.4 Air-sea CO_2 Flux

Air-sea CO_2 flux is calculated from daily averaged model data over 2001 to 2019 (Table 2). The GoM overall is a CO_2 sink with a mean flux rate of 0.62 mol C m^{-2} yr^{-1} (11.77 Tg C yr^{-1}), which is commensurate with the reported value of 11.8 Tg C yr^{-1} by Coble et al. (2010). The greatest carbon uptake rate occurs in winter (1.97 mol C m^{-2} yr^{-1}), while the weakest carbon uptake is present during fall (0.16 mol C m^{-2} yr^{-1}). The strongest carbon efflux is simulated in summer (-0.57 C m^{-2} yr^{-1}). On average, water in the NGoM acts as a sink throughout the years, and the water in the Open GoM acts as a weak source during summer (and fall for 2002, 2004, 2006, and 2009) and a sink during the rest of the year. The direction and magnitude of the air-sea exchange can be seen in Fig. 10, where a positive number indicates the ocean is a carbon sink. The NGoM is a very strong CO_2 sink year-round and Open GoM is a source of CO_2 during summer but a sink in the rest of the year (except during fall in a few years), as shown in Fig. 10(b). There are clear trends and patterns on multiyear CO_2 air-sea flux as shown in Fig. 10(a), where greater air-sea CO_2 flux average could be seen at the end of 2019 than that of 2001, resulting in a stronger carbon sink in both regions. A significant anomaly in the middle part of the record (2009-2011) can be observed, which could result from the influence of a large negative North Atlantic Oscillation (NAO) and El Niño in 2010 (Buchan et al., 2014). Similar observations in the Caribbean Sea are attributed to the single-year anomalies in the climate indices and the climate mode teleconnection (Wanninkhof et al., 2019).

In the last three rows of Table 2, the annual air-sea CO_2 flux is listed together with that reported by Xue et al. (2016) for 2005–2010, Robbins et al. (2014) for 1996-2012, and Gomez et al. (2020) for 2005–2014. In this study, the CO_2 air-sea flux is calculated with a timestep of 240 s, and output in the form of a daily average. The gas transfer velocity coefficient of 0.31 cm h^{-1} is used in Eq. (2). Using the same gas transfer velocity parameterization with this study, Xue et al. (2016) simulated a smaller carbon sink estimation in NGoM and a larger carbon sink estimation in the Open GoM due to their overestimation of shelf pCO_2 and underestimation of Open GoM pCO_2, which is likely resulted from the over-simplified prescription of the initial and boundary condition of DIC and TA (based on the empirical relationship with temperature and salinity). To compare with the flux estimates of Gomez, et al. (2020), we rescale our estimates to the gas transfer velocity parameterization used in their work (Wanninkhof, 2014) and produced mean estimations of 1.59, 0.52, 0.50 mol m^{-2} yr^{-1} for NGoM, Open GoM and Gulf-wide, respectively. Gomez et al. (2020) simulate smaller carbon sink values possibly due to the overestimation in NGoM shelf surface pCO_2 (especially near the MARS plume region and WF, the model-data discrepancy can be viewed in the supporting information Fig. S6 in their paper). The observation-based studies by Huang et al. (2015) yielded an annual sink of 0.96 ± 3.7 mol C m^{-2} yr^{-1}, based on the monthly satellite products QuikSCAT wind data (12.5 km resolution). Lohrenz et al. (2018) estimated an annual sink of 1.1 ± 0.3 mol C m^{-2} yr^{-1}, using gas transfer velocities estimated for each 8-day period. These two observation-based studies suggest a larger carbon sink than previous model work and are more consistent with the estimation of this work. Another reason that this study estimated a stronger air-sea flux is because previously reported values are based on an earlier timespan when the ocean was a weaker carbon sink due to a relatively low atmospheric pCO_2 compared with more current conditions. After comparing with multiple sources, we believe the air-sea CO_2 flux estimated in this work is more reliable than previous GoM model studies.

https://doi.org/10.5194/bg-2021-339
Preprint. Discussion started: 17 December 2021

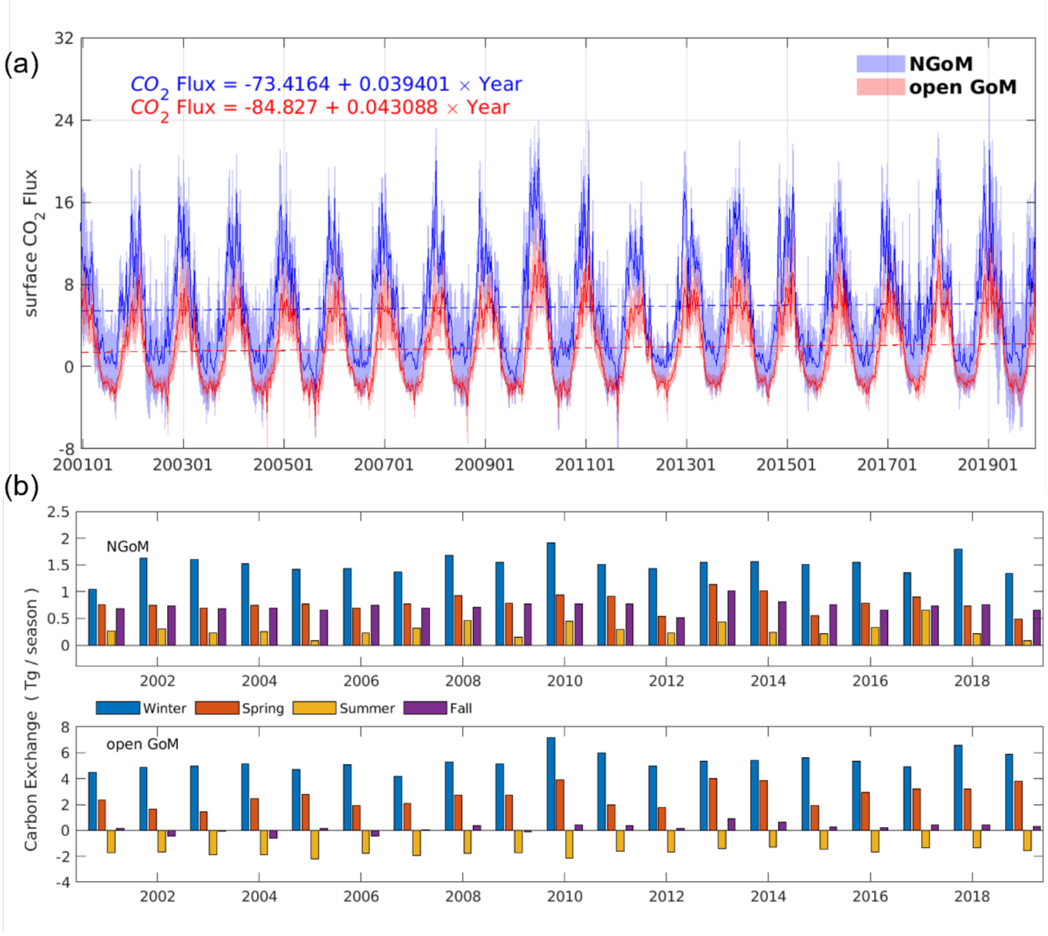

Figure 10: Air-sea CO_2 exchange over GoM: a) multiyear CO_2 flux regression over the weekly mean levels in NGoM and Open GoM; b) seasonal CO_2 air-sea exchange budget over two decades in NGoM and Open GoM.

Table 2. GoM air-sea CO_2 flux summary

		NGoM	Open GoM	Gulf wide
			mmol m^{-2} d $^{-1}$	
This work	Spring	4.93 ± 10.55	2.91 ± 1.35	2.48 ± 3.75
	Summer	1.71 ± 6.19	-1.83 ± 0.42	-1.55 ± 2.25
	Fall	4.79 ± 4.93	0.17 ± 1.04	0.45 ± 2.47
	Winter	10.00 ± 9.50	5.80 ± 2.24	5.40 ± 4.30
			mol m^{-2} yr $^{-1}$	
	Annual	1.96 ± 2.63	0.64 ± 0.42	0.62 ± 1.06
Xue et al., 2016	Annual	0.32±0.74	1.04±0.46	0.71±0.54
Robbins et al., 2014	Annual	0.44±0.37	0.48±0.07	0.19±0.08

Gomez et al., 2020	Annual	0.93±1.65	0.33±0.87	0.35±1.01

5 Discussion

In this study, we demonstrate that the regional high-resolution carbon model can reproduce the spatial and seasonal patterns of ocean surface pCO_2 and generate reliable TA/DIC profiles on the NGoM shelf. We have detected a consistent acidification trend in the GoM over the past two decades. In this session, we further diagnose river discharge and global ocean's impacts on the GoM carbon system via a comparison between the control experiment (His) and the two perturbed experiments (Bry and NoR), followed by a discussion of model uncertainty.

5.1 Contribution from River and Global Ocean

Two sets of perturbed experiments (Bry, NoR) are performed to complement the control experiment (His). One with the clamped boundary conditions that repeat the DIC and TA level as that of the year 2000, the other with the river forcing removed to examine the impact of fluvial input on the coastal carbon system. Figure 11 shows the multiyear averaged rate of change and mean levels of the four carbon variables (pCO_2, pH, Ω_{Arag}, and CO_2 flux) simulated by the three experiments. Table 3 summarizes the mean levels of pCO_2 over the NGoM and Open GoM. The definition of the pCO_2^{th}, the pCO_2^{nt}, the pCO_2^{GPP}, and the pCO_2^{flux} can be found in Sect. 4.1**.** The pCO_2^{mixing} is defined in Eq. (7), which reflects the pCO_2 level due to the heterogeneous water mixing. It can also be considered as the pCO_2 level determined by the water with a multiyear mean temperature and without the influence from gross primary production or air-sea CO_2 flux.

$$pCO_2^{nt} = pCO_2^{GPP} + pCO_2^{\text{flux}} + pCO_2^{\text{mixing}} \qquad (7)$$

The most salient difference among the three experiments is the significant elevation of annual mean pCO_2 level (in Fig. 11) in the NGoM during the NoR experiment, combined with a significantly reduced carbon sink during summer (in Fig. 12, from 0.287 to -0.093 Tg season^{-1} using His as a benchmark). The difference can be better resolved by the pCO_2 decomposition results shown in Table 3, where a drastic change in water carbon system emerges in NGoM during the NoR experiment (as compared to the other experiments with river input), evidenced by the large pCO_2^{mixing} value deviated from that of His and Bry experiment in the NGoM region during spring, summer, and winter. The low values of pCO_2^{nt} in NGoM during summer can be explained by a strong biological drawdown of CO_2 associated with the high productivity fuelled by riverine nutrient supply. A pCO_2^{GPP} component of -35.35 and -35.46 µatm corresponding to the strong biological drawdown of CO_2 in Bry and His experiments are in sharp contrast to that of the NoR experiment, which is only -3.10 µatm. Consequently, distinct patterns of CO_2 air-sea flux are shown in Fig. 12, and highly contrasting CO_2 air-sea flux-induced surface pCO_2 changes are shown in Table 3 (pCO_2^{flux}). The summer pCO_2^{flux} component for NGoM of the two experiments with river inputs exhibits a relatively large value (~ 43.5 µatm) compared with that of the NoR experiment (0.2 µatm), demonstrating much smaller disequilibrium between oceanic and atmospheric pCO_2 when rivers are absent. The changes introduced by removing the river showcase the

https://doi.org/10.5194/bg-2021-339
Preprint. Discussion started: 17 December 2021

dominating impact of river input to the NGoM carbon system in terms of gross primary production, surface pCO_2 level, and air-sea CO_2 exchange.

The Bry experiment is intended to resemble a GoM carbon system evolving with local carbon forcing without the influence of secondary carbon accumulation transported from the global ocean. From Fig. 11, we can see the directions (+/- signs) of the trend of all four carbon variables are preserved for all three experiments. This means under both perturbations, the regional ocean continued to have an acidifying tendency with increasing pCO_2, decreasing pH, decreasing Ω_{Arag}, and increasing CO_2 air-sea flux. This result is intuitively expected as the local atmospheric pCO_2 keeps increasing at a faster rate than that of the ocean, which should determine the direction of ocean carbon system change. Results from Table 3 show a close resemblance in the magnitude and seasonal pattern between Bry and His experiment in the Open GoM region, with a small yet steady reduction in pCO_2^{mixing} for the Bry experiment among all seasons. The small reductions in pCO_2^{mixing} of the Bry experiment compared to that of His reflect the contribution from extraneous carbon accumulation from the global ocean that is included in the His experiment. As expected, slightly greater CO_2 sink values are reported in Fig. 12 for Bry than His. Since the Bry experiment has a smaller carbon accumulation in the Open GoM region compared to that of the His experiment, the ocean surface requires a slightly greater carbon uptake to reach equilibrium with the atmosphere. The acidification trend results can be seen from Fig. 11(b), where intensified acidification trends are simulated for His experiment (-0.0015789 yr^{-1}) compared with that of Bry (-0.0015396 yr^{-1}) and NoR (-0.0015243 yr^{-1}). Combining the results from the three experiments, we conclude that, in addition to elevated atmospheric CO_2 level, both inputs from MARS and global oceans contribute to the overall acidification trend in GoM, with the impacts from MARS mainly limited to the NGoM shelf region and global ocean's impacts spanning in the Open GoM.

Table 3. Sea surface pCO_2 decomposition among experiments

	unit: *μatm*	NGoM			Open GoM		
		His	Bry	NoR	His	Bry	NoR
Spring	pCO_2^{th}	315.75	315.29	316.83	357.09	356.57	358.31
	pCO_2^{nt}	432.75	432.11	423.55	399.59	399.14	399.09
	pCO_2^{GPP}	-26.83	-26.79	-3.34	-2.95	-2.96	-2.64
	pCO_2^{flux}	56.83	57.41	49.24	3.41	3.46	3.46
	pCO_2^{mixing}	402.75	401.49	377.65	399.12	398.64	398.27
Summer	pCO_2^{th}	429.9	429.28	431.38	428.65	428.04	430.13
	pCO_2^{nt}	327.13	326.63	364.24	382.49	382.09	380.7
	pCO_2^{GPP}	-35.46	-35.35	-3.1	-3.44	-3.36	-2.09
	pCO_2^{flux}	43.41	43.57	0.2	-2.38	-2.34	-2.19

	pCO_2^{mixing}	319.18	318.41	367.14	388.31	387.79	384.97
Fall	pCO_2^{th}	374.01	373.47	375.3	406.92	406.34	408.32
	pCO_2^{nt}	353.69	353.43	358.06	370.78	370.54	370.28
	pCO_2^{GPP}	-13.64	-13.61	-1.72	-1.69	-1.63	-1.27
	pCO_2^{flux}	63.87	64.08	58.23	0.19	0.23	0.25
	pCO_2^{mixing}	303.47	302.97	301.56	372.28	371.94	371.29
Winter	pCO_2^{th}	270.51	270.12	271.44	340.54	340.06	341.72
	pCO_2^{nt}	458.11	457.77	432.23	393.35	392.79	393.45
	pCO_2^{GPP}	-8.01	-8.06	-1.88	-1.77	-1.82	-1.67
	pCO_2^{flux}	89.62	90.03	121.45	6.85	6.92	6.83
	pCO_2^{mixing}	376.5	375.8	312.65	388.27	387.7	388.29

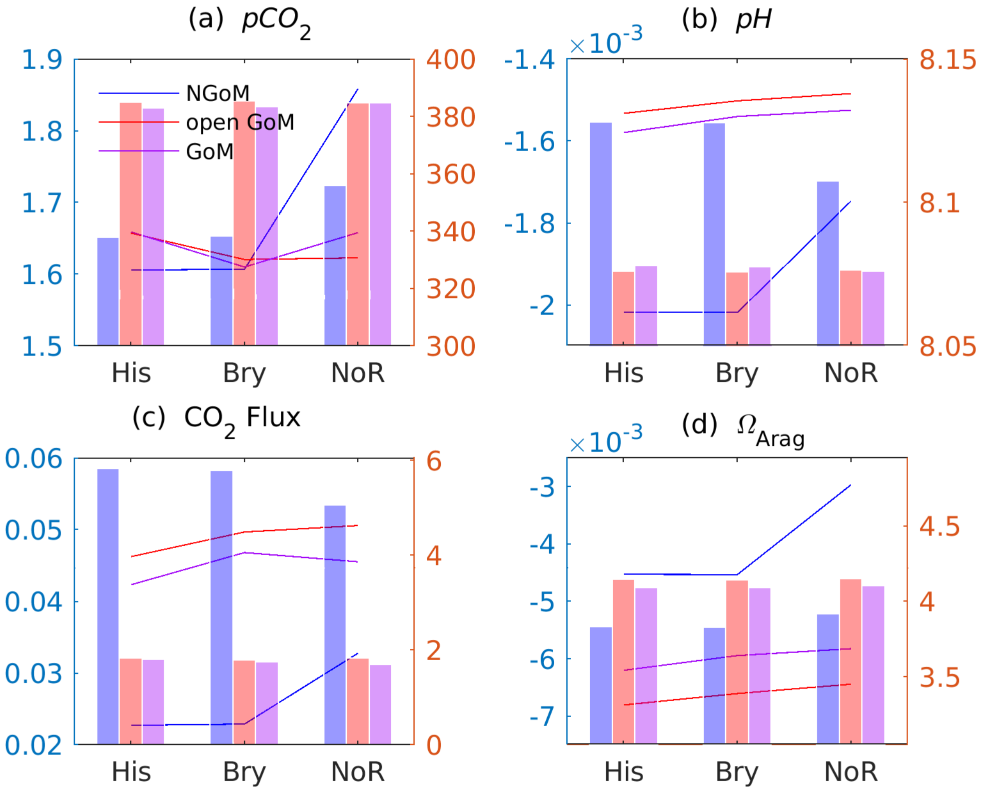

Figure 11: Multiyear synoptic of sea surface *pCO_2*, *pH*, CO_2 air-sea flux, Ω_{Arag} with His, Bry, and NoR experiment. Solid lines referring to the left axis denote the annual rate of change over 2001 to 2019, color bars referring to the right axis denote the mean level over 2001-2019. Color legend: blue – NGoM, red – Open GoM, purple – GoM wide for both the line plot and the bar plot. The unit for *pCO_2*, *pH*, CO_2 flux, and Ω_{Arag} are µatm, 1 (full scale), mmol m^{-2} d^{-1}, 1, respectively. (Noted that the CO_2 air-sea flux used ocean convention, where positive value indicate transport from air to sea, i.e. ocean is a sink)

A likely warmer climate combined with heavier precipitation and greater river discharge is predicted in the following years for MARS (Dai et al., 2020; Fischer & Knutti, 2015; Frei et al., 1998; Tao et al., 2014), although climate change might reduce precipitation for some low and middle latitudes regions (Arora & Boer, 2001; Na, Fu, & Kodama, 2020). A warmer climate will reduce the momentum of the Loop Current, and less tropic water (reduce by about 20–25%) will be introduced into the GoM from the Caribbean (Liu et al., 2012). As a consequence, Loop Current might penetrate less into the NGoM and reduce the upwelling along the NGoM and WF slope. Stronger river discharge with nutrient loads will exacerbate the NGoM acidification in bottom water (Laurent et al., 2018) while increasing the surface water biological CO_2 utilization and removal, creating larger river plume regions that exhibit distinct carbon footprint compared to its surrounding waters. Such predictions resemble the perturbation prescribed in the Bry and NoR experiments, where reduced global ocean impact can be assessed by the difference between Bry and His experiments, and impacts from increased river discharge can be assessed by the difference between His and NoR experiments. We anticipate the Open GoM to be a stronger carbon sink in the future under the projection of Loop Current weakening. And the NGoM will continue to be a strong carbon sink with the sink region expanded in response to predicted greater river discharge and smaller momentum in Loop Current.

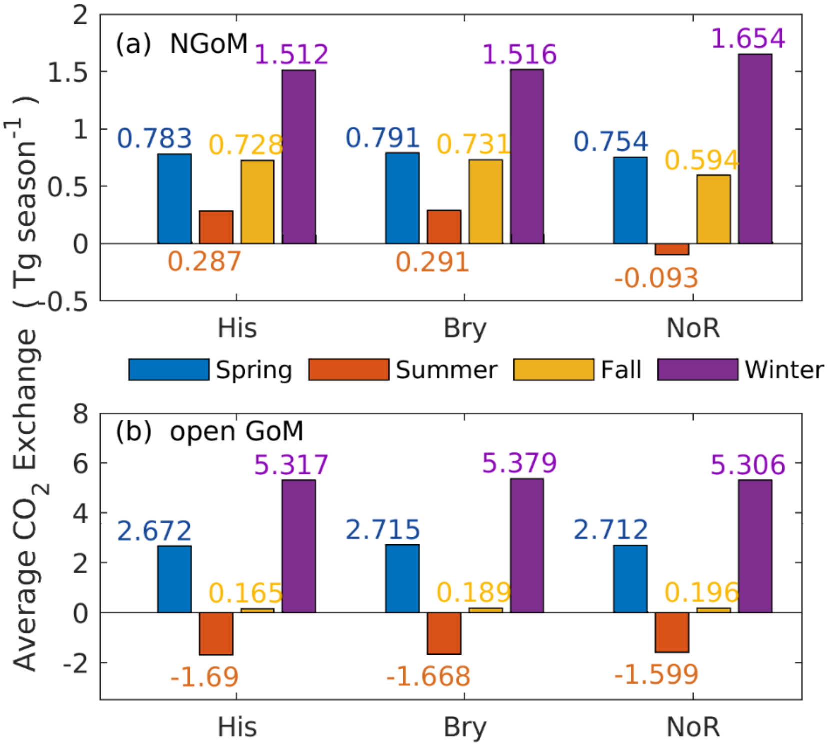

Figure 12: Seasonal air-sea CO_2 exchange at NGoM and Open GoM region among the His (historical), Bry (fixed boundary), and NoR (non-river) experiment.

5.2 Model-Data Discrepancy and Model Uncertainty

Field samples of the carbon system give us synoptic knowledge of the carbon cycle in the ocean. However, carbon system attributes are subject to large fluctuation due to temperature, salinity, mixing, and biological activities, current observations of the carbon system at the sea surface or vertically along transects are far from enough to reveal the carbon system evolution in the GoM. As ship-based observations are limited by the spatial coverage and temporal coverage, mooring observations have a high-frequency (~3 h) in time but only cover limited geological locations. ML model derived from remote sensing and cruise data inherit the bias from satellite ocean color products and ship-based measurements, and more importantly, it assumes the training data contains all information that defines the system it is trying to predict, which is not necessarily true. One benefit of the numerical models is to offer information to bridge fragmentary knowledge, fill in the gaps between observation and reality. However, the marine carbon cycle is admittedly a complex process. Several simplifications and parameterizations are needed to perform a numerical simulation. Nevertheless, specifications for some key processes may warrant further investigation and better parameterization: 1) The multiple alkalinity generation processes in the sediment pool in current experiments are linked linearly with the aerobic decomposition of PON with a fixed ratio, which can potentially induce large bias during high PON concentration. The anoxic zone chemistry component can be added to properly simulate the carbonate system in oxygen-deficient conditions (Raven, Keil, & Webb, 2021), which can prevail in bottom boundary layer waters in coastal regions in NGoM, especially during summer. Adding in anoxic zone chemistry will also allow a more diversified prescription for TA generation, which plays a key role in the understanding of sediment *pH* dynamics (Gustafsson et al. 2019; Middelburg, Soetaert & Hagens, 2020). 2) In our model, the density-related fragmentation/flocculation of detritus OM is simplified with one particulate and one dissolved pool, each with a fixed sinking rate. Coagulation and flocculation can transform DOC into particulate OM, or subsequently form large aggregates, whose remineralization rate can be much faster (Ploug et al., 1999). The remineralization-sinking dynamic determined the fate of OM decomposition (and water column DIC profile) and should be allowed to have more degree of freedom in future model development. 3) Calcification in this work can reflect the primary factors regulating marine calcification. However, important feedback from water acidity on the calcification is omitted due to the overall supersaturation with aragonite in GoM shelf waters. Therefore, the modeled $CaCO_3$/PON ratio could not reflect the decreasing trends of the $CaCO_3$/PON ratio under acidification (Zondervan et al., 2001). 4) Phytoplankton groups can play different roles in carbon cycling given their different sizes, sinking rates, calcification rates, etc., and their relative ratio would be critical to the carbon dynamic (Le Moigne et al. 2015; Poulton et al. 2007). The interplay between zooplankton grazing and phytoplankton bloom in this work captured the seasonal dynamic but only had fixed modes toward nutrient levels. High nutrient concentration favors the success of diatom, and lower nutrient level gives small phytoplankton a competitive advantage in NGoM (Aké-Castillo & Vázquez, 2008; Chakraborty & Lohrenz, 2015; Qian et al., 2003; Strom & Strom, 1996). More phytoplankton groups and possible predation avoidance mechanisms could be added to the model to give the bloom pattern (and subsequently the carbon export) more variance (Liszka, 2018; Rost & Riebesell, 2004). 5) Adding the higher trophic level biology could be the next step to improve the model. Marine fishes are reported to produce precipitated carbonates within their intestines at high rates and contribute to TA increase in the top 1000 meters of ocean waters (Wilson et al., 2009). 6) This model did not include sediment silicate weathering and carbon flux through atmospheric deposition, which can potentially be important sources/sinks of carbon to the ocean waters as well (Jurado et al., 2008; Wallmann et al. 2008).

https://doi.org/10.5194/bg-2021-339
Preprint. Discussion started: 17 December 2021

6 Conclusions

Building upon a Global Climate & Earth system model, the high-resolution regional carbon model can reliably simulate the spatial and temporal pattern of the surface ocean carbon system in the GoM. In this study, we show for the first time a solid validation of a regional carbon model via direct comparison against high-frequency CO_2 buoys, TA/DIC vertical profiles along the coastal transects, remote sensing-based ML model product, and underway pCO_2 measurements (surface). We calculated the decadal trends of important carbon system variables such as pCO_2, pH, air-sea CO_2 exchange, and Ω over the NGoM and Open GoM regions.

The GoM surface pCO_2 values experience a steady increase from 2001 to 2019, with an increasing rate of 1.61 µatm yr^{-1} in NGoM and 1.66 µatm yr^{-1} in Open GoM, respectively. Correspondingly, the ocean surface pH is declining at a rate of 0.0020 yr^{-1} and 0.0015 yr^{-1} for NGoM and Open GoM, respectively. The surface Ω over the NGoM and Open GoM region remain supersaturated with aragonite during the time span of the model but with a slightly decreasing trend. The carbon sink of both NGoM and Open GoM region have increasing trends and will continue to increase at a faster pace in the coming years under the prospect of climate change and the rising atmospheric pCO_2.

We decouple the influence on surface pCO_2 into thermal, nonthermal components and further analyze the surface pCO_2 changes due to gross primary production and air-sea CO_2 flux. We find that the low temperature during winter and the biological uptake during spring and summer are the primary drivers making GoM an overall CO_2 sink. During the modeled period of 2001-2009, the GoM overall is a CO_2 sink with a mean flux rate of 0.62 mol C m^{-2} yr^{-1} (11.77 Tg C yr^{-1}). The NGoM region is a CO_2 sink year-round and is very susceptible to changes in river forcing. The Open GoM region is dominated by thermal effects and converts from carbon sink to a source during summer.

Historical simulation (His) and perturbed tests (Bry, NoR) are performed to determine whether observed changes in the GoM carbon system are driven by secondary effects of carbon accumulation from the global ocean or local forcing such as river inputs. The results show that, in addition to the increasing atmospheric pCO_2 over the GoM, the spatial distribution and trend in carbon system variables could only be explained when the effects of carbon accumulation via boundary conditions and the impact from river discharge are included. With a projected warming climate, we anticipate the GoM to be a stronger carbon sink due to an elevated river discharge and reduced impact from the global ocean.

Code/Data availability:

Author contribution: Z. George Xue designed the experiments and Le Zhang carried them out. Le Zhang developed the model code and performed the simulations. Le Zhang and Z. George Xue prepared the manuscript.

Competing interests: The authors declare that they have no conflict of interest.

Acknowledgment: Research support provided through the National Science Foundation (award number OCE-1635837; EnvS 1903340; OCE- 2049047; OCE-2054935), NASA (award number NNH17ZHA002C), Louisiana Board of Regents (award number NASA/LEQSF (2018-20)-Phase3-11), NOAA Graduate Research Fellowship in Ocean, Coastal and Estuarine Acidification (OA R/CWQ-11). Computational support was provided by the High-Performance Computing Facility (clusters SuperMIC and QueenBee3) at Louisiana State University. Calculated CO_2 flux data is available at the LSU mass storage system and details are on the webpage of the Coupled Ocean Modeling Group at LSU (http://coastandenvironment.lsu.edu/docs/faculty/xuelab/). Data requests can be sent to the corresponding author via this webpage.

References

Adkins, J. F., Naviaux, J. D., Subhas, A. V., Dong, S., & Berelson, W. M. (2021). The Dissolution Rate of CaCO3 in the Ocean. *Annual Review of Marine Science*, *13*, 57–80. https://doi.org/10.1146/annurev-marine-041720-092514

Aké-Castillo, J. A., & Vázquez, G. (2008). Phytoplankton variation and its relation to nutrients and allochthonous organic matter in a coastal lagoon on the Gulf of Mexico. *Estuarine, Coastal and Shelf Science*, *78*(4), 705–714.

Anav, A., Friedlingstein, P., Kidston, M., Bopp, L., Ciais, P., Cox, P., … Zhu, Z. (2013). Evaluating the land and ocean components of the global carbon cycle in the CMIP5 earth system models. *Journal of Climate*, *26*(18), 6801–6843. https://doi.org/10.1175/JCLI-D-12-00417.1

Arora, V. K., & Boer, G. J. (2001). Effects of simulated climate change on the hydrology of major river basins. *Journal of Geophysical Research: Atmospheres*, *106*(D4), 3335–3348. https://doi.org/10.1029/2000JD900620

Barbero, L., Pierrot, D., Wanninkhof, R., Baringer, M. O., Byrne, R. H., Langdon, C., … Stauffer, B. A. (2019). Dissolved inorganic carbon, total alkalinity, nutrients, and other variables collected from CTD profile, discrete bottle, and surface underway observations using CTD, Niskin bottle, flow-through pump, and other instruments from NOAA Ship Ronald H. Brown i. *NOAA National Centers for Environmental Information. Dataset. Https://Doi.Org/10.25921/Yy5k-Dw60*, [Accessed 2021-05-24].

Booij, N., Ris, R. C., & Holthuijsen, L. H. (1999). A third-generation wave model for coastal regions: 1. Model description and validation. *Journal of Geophysical Research: Oceans*, *104*(C4), 7649–7666.

Boscolo-Galazzo, Flavia, K. A., Crichton, A. R., Mawbey, E. M., Wade, B. S., & Pearson, P. N. (2021). Temperature controls carbon cycling and biological evolution in the ocean twilight zone. *Science*, *371*(6534), 1148–1152. DOI: 10.1126/science.abb6643

Boyd, P. W., Claustre, H., Levy, M., Siegel, D. A., & Weber, T. (2019). Multi-faceted particle pumps drive carbon sequestration in the ocean. *Nature*, *568*(7752), 327–335. https://doi.org/10.1038/s41586-019-1098-2

Boyer, T. P., García, H. E., Locarnini, R. A.; Zweng, M. M., Mishonov, A. V., Reagan, J. R., Weathers, K. A., Baranova, O. K., Paver, C. R.; Seidov, D., Smolyar, I. V. (2018). World Ocean Atlas 2018. [woa18_all_o16_01.nc]. NOAA National Centers for Environmental Information. Dataset. https://www.ncei.noaa.gov/archive/accession/NCEI-WOA18. Accessed 2020-10-01.

Buchan, J., Hirschi, J. J.-M., Blaker, A. T., & Sinha, B. (2014). North Atlantic SST anomalies and the cold North European weather events of winter 2009/10 and December 2010. *Monthly Weather Review*, *142*(2), 922–932. https://doi.org/10.1175/MWR-D-13-00104.1

Buesseler, K. O., Boyd, P. W., Black, E. E., & Siegel, D. A. (2020). Metrics that matter for assessing the ocean biological carbon pump. *Proceedings of the National Academy of Sciences*, *117*(18), 9679–9687. https://doi.org/10.1073/pnas.1918114117

Burton, E. A., & Walter, L. M. (1987). Relative precipitation rates of aragonite and Mg calcite from seawater: Temperature or carbonate ion control?. *Geology*, *15*(2), 111-114. https://doi.org/10.1130/0091-7613(1987)15%3C111:RPROAA%3E2.0.CO;2

Bushinsky, S. M., Landschützer, P., Rödenbeck, C., Gray, A. R., Baker, D., Mazloff, M. R., … Sarmiento, J. L. (2019). Reassessing Southern Ocean Air-Sea CO2 Flux Estimates With the Addition of Biogeochemical Float Observations. *Global Biogeochemical Cycles*, *33*(11), 1370–1388. https://doi.org/10.1029/2019GB006176

Cai, W. J., Hu, X., Huang, W. J., Murrell, M. C., Lehrter, J. C., Lohrenz, S. E., … Gong, G. C. (2011). Acidification of subsurface coastal waters enhanced by eutrophication. *Nature Geoscience*, *4*(11), 766–770. https://doi.org/10.1038/ngeo1297

Chassignet, E. P., Smith, L. T., Halliwell, G. R., & Bleck, R. (2003). North Atlantic simulations with the Hybrid Coordinate Ocean Model (HYCOM): Impact of the vertical coordinate choice, reference pressure, and thermobaricity. *Journal of Physical Oceanography*, 33(12), 2504-2526. https://doi.org/10.1175/1520-0485(2003)033%3C2504:NASWTH%3E2.0.CO; 2

Chakraborty, S., & Lohrenz, S. E. (2015). Phytoplankton community structure in the river-influenced continental margin of the northern Gulf of Mexico. *Marine Ecology Progress Series*, *521*, 31–47. https://doi.org/10.3354/meps11107

Chen, S., Hu, C., Barnes, B. B., Wanninkhof, R., Cai, W. J., Barbero, L., & Pierrot, D. (2019). A machine learning approach to estimate surface ocean pCO2 from satellite measurements. *Remote Sensing of Environment*, *228*(April), 203–226. https://doi.org/10.1016/j.rse.2019.04.019

Chen, X., Lohrenz, S. E., & Wiesenburg, D. A. (2000). Distribution and controlling mechanisms of primary production on the Louisiana–Texas continental shelf. *Journal of Marine Systems*, *25*(2), 179–207. https://doi.org/10.1016/S0924-7963(00)00014-2

Coble, P. G., Robbins, L. L., Daly, K. L., Cai, W. J., Fennel, K., & Lorenz, S. E. (2010). A preliminary carbon budget for the Gulf of Mexico. *Ocean Carbon and Biogeochemistry Newsletter*, *3*(3), 1.

Czerny, J., Schulz, K. G., Ludwig, A., & Riebesell, U. (2013). Technical Note : A simple method for air – sea gas exchange measurements in mesocosms and its application in carbon budgeting. *Biogeosciences*, *10*, 1379–1390. https://doi.org/10.5194/bg-10-1379-2013

Dai, A., Rasmussen, R. M., Liu, C., Ikeda, K., & Prein, A. F. (2020). A new mechanism for warm-season precipitation response to global warming based on convection-permitting simulations. *Climate Dynamics*, *55*(1), 343–368. https://doi.org/10.1007/s00382-017-3787-6

Danabasoglu, G. (2019). NCAR CESM2-WACCM-FV2 model output prepared for CMIP6 CMIP historical， Version 2019. *Earth System Grid Federation*, https://doi.org/10.22033/ESGF/CMIP6.11298.

Davis, C. E., Blackbird, S., Wolff, G., Woodward, M., & Mahaffey, C. (2019). Seasonal organic matter dynamics in a temperate shelf sea. *Progress in Oceanography*, *177*, 101925. https://doi.org/10.1016/j.pocean.2018.02.021

Delgado, J. A., Sudre, J., Tanahara, S., Montes, I., Hernández-Ayón, J. M., & Zirino, A. (2019). Effect of Caribbean Water incursion into the Gulf of Mexico derived from absolute dynamic topography, satellite data, and remotely sensed chlorophyll a. *Ocean Science*, *15*(6), 1561-1578. https://doi.org/10.5194/os-15-1561-2019

DeVries, T., Le Quéré, C., Andrews, O., Berthet, S., Hauck, J., Ilyina, T., … Séférian, R. (2019). Decadal trends in the ocean carbon sink. *Proceedings of the National Academy of Sciences of the United States of America*, *116*(24), 11646–11651. https://doi.org/10.1073/pnas.1900371116

Dickson, A. G. (1981). An exact definition of total alkalinity and a procedure for the estimation of alkalinity and total inorganic carbon from titration data. *Deep Sea Research Part A. Oceanographic Research Papers*, *28*(6), 609-623. https://doi.org/10.1016/0198-0149(81)90121-7

Dickson, A. G., Sabine, C. L., & Christian, J. R. (2007). Guide to best practices for ocean CO2 measurements. North Pacific Marine Science Organization.

Dils, B., Buchwitz, M., Reuter, M., Schneising, O., Boesch, H., Parker, R., ... & Wunch, D. (2014). The Greenhouse Gas Climate Change Initiative (GHG-CCI): comparative validation of GHG-CCI SCIAMACHY/ENVISAT and TANSO-FTS/GOSAT CO 2 and CH 4 retrieval algorithm products with measurements from the TCCON. *Atmospheric Measurement Techniques*, *7*(6), 1723-1744. https://doi.org/10.5194/amt-7-1723-2014

Doney, S. C., Fabry, V. J., Feely, R. A., & Kleypas, J. A. (2009). Ocean acidification: The other CO2 problem. *Annual Review of Marine Science*, *1*, 169–192. https://doi.org/10.1146/annurev.marine.010908.163834

Dzwonkowski, B., Fournier, S., Reager, J. T., Milroy, S., Park, K., Shiller, A. M., … Sanial., V. (2018). Tracking sea surface salinity and dissolved oxygen on a river-influenced, seasonally stratified shelf, Mississippi Bight, northern Gulf of Mexico.

Continental Shelf Research, *169*, 25–33. https://doi.org/10.1016/j.csr.2018.09.009

Eccles, R., Zhang, H., & Hamilton, D. (2019). A review of the effects of climate change on riverine flooding in subtropical and tropical regions. *Journal of Water and Climate Change*, *10*(4), 687–707. https://doi.org/10.2166/wcc.2019.175

Eyring, V., Bony, S., Meehl, G. A., Senior, C. A., Stevens, B., Stouffer, R. J., & Taylor, K. E. (2016). Overview of the Coupled Model Intercomparison Project Phase 6 (CMIP6) experimental design and organization. *Geoscientific Model Development*, *9*(5), 1937-1958. https://doi.org/10.5194/gmd-9-1937-2016

Farmer, J. R., Hertzberg, J. E., Cardinal, D., Fietz, S., Hendry, K., Jaccard, S. L., … Al, E. (2021). Assessment of C, N, and Si isotopes as tracers of past ocean nutrient and carbon cycling. *Global Biogeochemical Cycles*, *35*(7), e2020GB006775. https://doi.org/10.1029/2020GB006775

Feely, R. A., Doney, S. C., & Cooley, S. R. (2009). Ocean acidification: Present conditions and future changes in a high-CO_2 world. *Oceanography*, *22*(4), 36–47. https://www.jstor.org/stable/24861022

Feely, R. A., Sabine, C. L., Lee, K., Millero, F. J., Lamb, M. F., Greeley, D., … Wong, C. S. (2002). In situ calcium carbonate dissolution in the Pacific Ocean. *Global Biogeochemical Cycles*, *16*(4), 91–1. https://doi.org/10.1029/2002GB001866

Fennel, W. (2008). Towards bridging biogeochemical and fish-production models. *Journal of Marine Systems*, *71*(1-2), 171-194.

Fennel, K., Wilkin, J., Levin, J., Moisan, J., O'Reilly, J., & Haidvogel, D. (2006). Nitrogen cycling in the Middle Atlantic Bight: Results from a three-dimensional model and implications for the North Atlantic nitrogen budget. *Global Biogeochemical Cycles*, *20*(3), 1–14. https://doi.org/10.1029/2005GB002456

Fennel, K., Wilkin, J., Previdi, M., & Najjar, R. (2008). Denitrification effects on air-sea CO2 flux in the coastal ocean: Simulations for the northwest North Atlantic. *Geophysical Research Letters*, *35*(24), 1–5. https://doi.org/10.1029/2008GL036147

Fennel, K., & Wilkin, J. (2009). Quantifying biological carbon export for the northwest North Atlantic continental shelves. *Geophysical Research Letters*, *36*(18), 2–5. https://doi.org/10.1029/2009GL039818

Fennel, K., Hetland, R., Feng, Y., & Dimarco, S. (2011). A coupled physical-biological model of the Northern Gulf of Mexico shelf: Model description, validation and analysis of phytoplankton variability. *Biogeosciences*, *8*(7), 1881–1899. https://doi.org/10.5194/bg-8-1881-2011

Fischer, E. M., & Knutti, R. (2015). Anthropogenic contribution to global occurrence of heavy-precipitation and high-temperature extremes. *Nature Climate Change*, *5*(6), 560–564. DOI: 10.1038/nclimate2617

Frei, C., Schär, C., Lüthi, D., & Davies, H. C. (1998). Heavy precipitation processes in a warmer climate. *Geophysical Research Letters*, *25*(9), 1431–1434. https://doi.org/10.1029/98GL51099

García, H. E., K. Weathers, C. R. Paver, I. Smolyar, T. P. Boyer, R. A. Locarnini, M. M. Zweng, A. V. Mishonov, O. K. Baranova, D. Seidov, and J. R. Reagan, (2019). World Ocean Atlas 2018, Volume 3: Dissolved Oxygen, Apparent Oxygen Utilization, and Oxygen Saturation. A. Mishonov Technical Ed.; NOAA Atlas NESDIS 83, 38 pp.

Gomez, F. A., Wanninkhof, R., Barbero, L., Lee, S. K., & Hernandez, F. J. (2020). Seasonal patterns of surface inorganic carbon system variables in the Gulf of Mexico inferred from a regional high-resolution ocean biogeochemical model. *Biogeosciences*, *17*(6), 1685–1700. https://doi.org/10.5194/bg-17-1685-2020

Gustafsson, E., Hagens, M., Sun, X., Reed, D. C., Humborg, C., Slomp, C. P., & Gustafsson, B. G. (2019). Sedimentary alkalinity generation and long-term alkalinity development in the Baltic Sea. *Biogeosciences*, *16*(2), 437-456. https://doi.org/10.5194/bg-16-437-2019

Haidvogel, D. B., Arango, H., Budgell, W. P., Cornuelle, B. D., Curchitser, E., Di Lorenzo, E., … Wilkin, J. (2008). Ocean forecasting in terrain-following coordinates: Formulation and skill assessment of the Regional Ocean Modeling System. *Journal of Computational Physics*, *227*(7), 3595–3624. https://doi.org/10.1016/j.jcp.2007.06.016

Ho, D. T., Law, C. S., Smith, M. J., Schlosser, P., Harvey, M., & Hill, P. (2006). Measurements of air-sea gas exchange at high wind speeds in the Southern Ocean: Implications for global parameterizations. *Geophysical Research Letters*, *33*(16). https://doi.org/10.1029/2006GL026817

Hofmann, E. E., Cahill, B., Fennel, K., Friedrichs, M. A. M., Hyde, K., Lee, C., … Xue, J. (2011). Modeling the dynamics of continental shelf carbon. *Annual Review of Marine Science*, *3*, 93–122. https://doi.org/10.1146/annurev-marine-120709-142740

Holligan, P. M., & Robertson, J. E. (1996). Significance of ocean carbonate budgets for the global carbon cycle. *Global Change Biology*, *2*(2), 85–95. https://doi.org/10.1111/j.1365-2486.1996.tb00053.x

Hu, X., & Cai, W. J. (2011). An assessment of ocean margin anaerobic processes on oceanic alkalinity budget. *Global Biogeochemical Cycles*, *25*(3). https://doi.org/10.1029/2010GB003859

Huang, W. J., Cai, W. J., Wang, Y., Lohrenz, S. E., & Murrell, M. C. (2015). The carbon dioxide system on the Mississippi River-dominated continental shelf in the northern Gulf of Mexico. *Journal of Geophysical Research: Oceans*, *120*(3), 1429–1445. https://doi.org/10.1002/2014JC010498

Inskeep, W. P., & Bloom, P. R. (1985). An evaluation of rate equations for calcite precipitation kinetics at pCO2 less than 0.01 atm and pH greater than 8. *Geochimica et Cosmochimica Acta*, *49*(10), 2165-2180. https://doi.org/10.1016/0016-7037(85)90074-2

Irigoien, X., Flynn, K. J., & Harris, R. P. (2005). Phytoplankton blooms: a 'loophole' in microzooplankton grazing impact? *Journal of Plankton Research*, *27*(4), 313–321. https://doi.org/10.1093/plankt/fbi011

Jiang, Z. P., Cai, W. J., Chen, B., Wang, K., Han, C., Roberts, B. J., … Li, Q. (2019). Physical and Biogeochemical Controls on pH Dynamics in the Northern Gulf of Mexico During Summer Hypoxia. *Journal of Geophysical Research: Oceans*, *124*(8), 5979–5998. https://doi.org/10.1029/2019JC015140

Jones, C. D., Arora, V., Friedlingstein, P., Bopp, L., Brovkin, V., Dunne, J., … Zaehle, S. (2016). C4MIP-The Coupled Climate-Carbon Cycle Model Intercomparison Project: Experimental protocol for CMIP6. *Geoscientific Model Development*, *9*(8), 2853–2880. https://doi.org/10.5194/gmd-9-2853-2016

Jurado, E., Dachs, J., Duarte, C. M., & Simo, R. (2008). Atmospheric deposition of organic and black carbon to the global oceans. *Atmospheric Environment*, *42*(34), 7931–7939. https://doi.org/10.1016/j.atmosenv.2008.07.029

King, A. L., Jenkins, B. D., Wallace, J. R., Liu, Y., Wikfors, G. H., Milke, L. M., & Meseck, S. L. (2015). Effects of CO2 on growth rate, C: N: P, and fatty acid composition of seven marine phytoplankton species. *Marine Ecology Progress Series*, *537*, 59–69. https://doi.org/10.3354/meps11458

Kishi, Michio J., Kashiwai, M., Ware, D. M., Megrey, B. A., Eslinger, D. L., Werner, F. E., … Zvalinsky, V. I. (2007). NEMURO-a lower trophic level model for the North Pacific marine ecosystem. *Ecological Modelling*, *202*(1–2), 12–25. https://doi.org/10.1016/j.ecolmodel.2006.08.021

Kishi, M. J., Ito, S. I., Megrey, B. A., Rose, K. A., & Werner, F. E. (2011). A review of the NEMURO and NEMURO. FISH models and their application to marine ecosystem investigations. *Journal of Oceanography*, *67*(1), 3–16. DOI: 10.1007/s10872-011-0009-4

Laurent, A., Fennel, K., Cai, W. J., Huang, W. J., Barbero, L., & Wanninkhof, R. (2017). Eutrophication-induced acidification of coastal waters in the northern Gulf of Mexico: Insights into origin and processes from a coupled physical-biogeochemical model. *Geophysical Research Letters*, *44*(2), 946–956. https://doi.org/10.1002/2016GL071881

Laurent, A., Fennel, K., Ko, D. S., & Lehrter, J. (2018). Climate change projected to exacerbate impacts of coastal eutrophication in the northern Gulf of Mexico. *Journal of Geophysical Research: Oceans*, *123*(5), 3408–3426. https://doi.org/10.1002/2017JC013583

Laurent, A., Fennel, K., & Kuhn, A. (2021). An observation-based evaluation and ranking of historical Earth system model simulations in the northwest North Atlantic Ocean. *Biogeosciences*, *18*(5), 1803–1822. https://doi.org/10.5194/bg-18-1803-2021

Lauvset, S. K., Carter, B. R., Perez, F. F., Jiang, L. Q., Feely, R. A., Velo, A., & Olsen, A. (2020). Processes Driving Global Interior Ocean pH Distribution. *Global Biogeochemical Cycles*, *34*(1), 1–17. https://doi.org/10.1029/2019GB006229

Le Moigne, F. A., Poulton, A. J., Henson, S. A., Daniels, C. J., Fragoso, G. M., Mitchell, E., ... & Zubkov, M. (2015). Carbon export efficiency and phytoplankton community composition in the A tlantic sector of the A rctic O cean. *Journal of Geophysical Research: Oceans*, *120*(6), 3896-3912. https://doi.org/10.1002/2015JC010700

Le Quéré, C., Andrew, R. M., Friedlingstein, P., Sitch, S., Pongratz, J., Manning, A. C., … Zhu, D. (2018). Global Carbon Budget 2018. *Earth System Science Data Discussions*, *10*(4), 2141–2194. https://doi.org/10.5194/essd-10-2141-2018

Lewis, E. R., & Wallace, D. W. R. (1998). *Program developed for CO2 system calculations* (No. cdiac: CDIAC-105). Environmental System Science Data Infrastructure for a Virtual Ecosystem. doi:10.15485/1464255.Liao, H., Yu, Y. yong, Wang, C., Han, X., & Song, Z. (2020). An explanation for the simulated aborted ENSO events in climate models. *Earth and Space Science Open Archive*. https://doi.org/10.1002/essoar.10502531.1

Lindsay, K., Bonan, G. B., Doney, S. C., Hoffman, F. M., Lawrence, D. M., Long, M. C., … Thornton, P. E. (2014). Preindustrial-control and twentieth-century carbon cycle experiments with the Earth system model CESM1(BGC). *Journal of Climate*, *27*(24), 8981–9005. https://doi.org/10.1175/JCLI-D-12-00565.1

Liu, Y., Lee, S. K., Muhling, B. A., Lamkin, J. T., & Enfield, D. B. (2012). Significant reduction of the Loop Current in the 21st century and its impact on the Gulf of Mexico. *Journal of Geophysical Research: Oceans*, *117*(C5). https://doi.org/10.1029/2011JC007555

Liu, Y., Lee, S. K., Enfield, D. B., Muhling, B. A., Lamkin, J. T., Muller-Karger, F. E., & Roffer, M. A. (2015). Potential impact of climate change on the Intra-Americas Sea: Part-1. A dynamic downscaling of the CMIP5 model projections. *Journal of Marine Systems*, *148*, 56–69. https://doi.org/10.1016/j.jmarsys.2015.01.007

Liszka, C. (2018). *Zooplankton-mediated carbon flux in the Southern Ocean: influence of community structure, metabolism and behaviour* (Doctoral dissertation, University of East Anglia).

Lohrenz, S. E., Cai, W. J., Chakraborty, S., Huang, W. J., Guo, X., He, R., … Tian, H. (2018a). Satellite estimation of coastal pCO2 and air-sea flux of carbon dioxide in the northern Gulf of Mexico. *Remote Sensing of Environment*, *207*, 71–83. https://doi.org/10.1016/j.rse.2017.12.039

Mackenzie, F. T., Lerman, A., & Andersson, A. J. (2004). Past and present of sediment and carbon biogeochemical cycling model. *Biogeosciences*, *1*(1), 11–32. https://doi.org/10.5194/bg-1-11-2004

Maher, D. T., & Eyre, B. D. (2012). Carbon budgets for three autotrophic Australian estuaries: Implications for global estimates of the coastal air-water CO 2 flux. *Global Biogeochemical Cycles*, *26*(1). https://doi.org/10.1029/2011GB004075

Mari, X., Passow, U., Migon, C., Burd, A. B., & Legendre, L. (2017). Transparent exopolymer particles: Effects on carbon cycling in the ocean. *Progress in Oceanography*, *151*(13–37). https://doi.org/10.1016/j.pocean.2016.11.002

Middelburg, J. J., Soetaert, K., & Hagens, M. (2020). Ocean alkalinity, buffering and biogeochemical processes. *Reviews of Geophysics*, *58*(3), e2019RG000681. https://doi.org/10.1029/2019RG000681

Millero, F. J. (1982). The effect of pressure on the solubility of minerals in water and seawater. *Geochimica et Cosmochimica Acta*, *46*(1), 11–22. https://doi.org/10.1016/0016-7037(82)90286-1

Millero, F. J. (1995). Thermodynamics of the carbon dioxide system in the oceans. *Geochimica et Cosmochimica Acta*, *59*(4), 661–677. https://doi.org/10.1016/0016-7037(94)00354-O

Millero, F. J. (2007). The marine inorganic carbon cycle. *Chemical Reviews*, *107*(2), 308–341. https://doi.org/10.1021/cr0503557

Millero, F. J. (2010). Carbonate constants for estuarine waters. *Marine and Freshwater Research*, *61*(2), 139–142.

Milliman, J. D., Troy, P. J., Balch, W. M., Adams, A. K., Li, Y. H., & Mackenzie, F. T. (1999). Biologically mediated dissolution of calcium carbonate above the chemical lysocline? *Deep Sea Research Part I: Oceanographic Research Papers*, *46*(10), 1653–1669. https://doi.org/10.1016/S0967-0637(99)00034-5

Moore, J. K., Doney, S. C., & Lindsay, K. (2004). Upper ocean ecosystem dynamics and iron cycling in a global three-dimensional model. *Global Biogeochemical Cycles*, *18*(4). https://doi.org/10.1029/2004GB002220

Mucci, A. (1983). The Solubility of Calcite and Aragonite in Seawater at Various Salinities, Temperatures and One Atmosphere Total Pressure. *American Journal of Science*, Vol. 283, pp. 780–799. https://doi.org/10.2475/ajs.283.7.780

Na, Y., Fu, Q., & Kodama, C. (2020). Precipitation probability and its future changes from a global cloud-resolving model and CMIP6 simulations. *Journal of Geophysical Research: Atmospheres*, *125*(5), e2019JD031926. https://doi.org/10.1029/2019JD031926

Najjar, R. G., Herrmann, M., Alexander, R., Boyer, E. W., Burdige, D. J., Butman, D., … Zimmerman, R. C. (2018). Carbon Budget of Tidal Wetlands, Estuaries, and Shelf Waters of Eastern North America. *Global Biogeochemical Cycles*, *32*(3), 389–416. https://doi.org/10.1002/2017GB005790

Ollila, A. (2020). Analysis of the Simulation Results of Three Carbon Dioxide (CO2) Cycle Models. *Physical Science International Journal*, *23*(4), 1–19. https://doi.org/10.9734/psij/2019/v23i430168

Orr, J., Najjar, R., Sabine, C. L., & Joos, F. (1999). Abiotic-howto. *Internal OCMIP Report*, *LSCE/CEA S.*

Orr, J., Najjar, R. G., Aumont, O., Bopp, L., Bullister, J. L., Danabasoglu, G., … Yool, A. (2017). Biogeochemical protocols and diagnostics for the CMIP6 Ocean Model Intercomparison Project (OMIP). *Geoscientific Model Development*, *10*(6), 2169–2199. https://doi.org/10.5194/gmd-10-2169-2017

Ploug, H., Grossart, H. P., Azam, F., & Jørgensen, B. B. (1999). Photosynthesis, respiration, and carbon turnover in sinking marine snow from surface waters of Southern California Bight: implications for the carbon cycle in the ocean. *Marine Ecology Progress Series*, *179*, 1–11. doi:10.3354/meps179001

Poulton, A. J., Adey, T. R., Balch, W. M., & Holligan, P. M. (2007). Relating coccolithophore calcification rates to phytoplankton community dynamics: Regional differences and implications for carbon export. *Deep Sea Research Part II:*

Topical Studies in Oceanography, *54*(5-7), 538-557. https://doi.org/10.1016/j.dsr2.2006.12.003

Qian, Y., Jochens, A. E., Kennicutt Ii, M. C., & Biggs, D. C. (2003). Spatial and temporal variability of phytoplankton biomass and community structure over the continental margin of the northeast Gulf of Mexico based on pigment analysis. *Continental Shelf Research*, *23*(1), 1–17. https://doi.org/10.1016/S0278-4343(02)00173-5

Raven, J. A., & Giordano, M. (2009). Biomineralization by photosynthetic organisms: Evidence of coevolution of the organisms and their environment? *Geobiology*, *7*(2), 140–154. https://doi.org/10.1111/j.1472-4669.2008.00181.x

Raven, M. R., Keil, R. G., & Webb, S. M. (2021). Microbial sulfate reduction and organic sulfur formation in sinking marine particles. *Science*, *371*(6525), 178–181. DOI: 10.1126/science.abc6035

Regnier, P., Friedlingstein, P., Ciais, P., Mackenzie, F. T., Gruber, N., Janssens, I. A., … Thullner, M. (2013). Anthropogenic perturbation of the carbon fluxes from land to ocean. *Nature Geoscience*, *6*(8), 597–607. https://doi.org/10.1038/ngeo1830

Reiman, J. H., & Xu, Y. J. (2019). Dissolved carbon export and CO2 outgassing from the lower Mississippi River – Implications of future river carbon fluxes. *Journal of Hydrology*, *578*(July), 124093. https://doi.org/10.1016/j.jhydrol.2019.124093

Renforth, P., & Henderson, G. (2017). Assessing ocean alkalinity for carbon sequestration. *Reviews of Geophysics*, *55*(3), 636–674. https://doi.org/10.1002/2016RG000533

Riebesell, U., Zondervan, I., Rost, B., Tortell, P. D., Zeebe, R. E., & Morel, F. M. (2000). Reduced calcification of marine plankton in response to increased atmospheric CO2. *Nature*, *407*(6802), 364–367.

Robbins, L. L., Daly, K. L., Barbero, L., Wanninkhof, R., He, R., Zong, H., … Smith, C. G. (2018). Spatial and Temporal Variability of pCO2, Carbon Fluxes, and Saturation State on the West Florida Shelf. *Journal of Geophysical Research: Oceans*, *123*(9), 6174–6188. https://doi.org/10.1029/2018JC014195

Robbins, L. L., Wanninkhof, R., Barbero, L., Hu, X., Mitra, S., Yvon-Lewis, S., … and Ryerson, T. (2014). Air-Sea Exchange, Report of The U.S. Gulf of Mexico Carbon Cycle Synthesis Workshop. *Ocean Carbon and Biogeochemistry Program and North American Carbon Program*, 66.

Robertson, R., & Hartlipp, P. (2017). Surface wind mixing in the regional ocean modeling system (ROMS). *Geoscience Letters*, *4*(1), 1–11. DOI 10.1186/s40562-017-0090-7

Rost, B., & Riebesell, U. (2004). Coccolithophores and the biological pump: responses to environmental changes. *Coccolithophores*, *Springer,* 99–125. DOI: 10.1007/978-3-662-06278-4_5

Saha, S., et al. (2010), NCEP Climate Forecast System Reanalysis (CFSR) Selected Hourly Time-Series Products, January 1979 to December 2010, https://doi.org/10.5065/D6513W89, *Research Data Archive at the National Center for Atmospheric Research, Computational and Information Systems Laboratory*, Boulder, Colo. Accessed 22 Oct 2020.

Saha, S., et al. (2011), NCEP Climate Forecast System Version 2 (CFSv2) 6-hourly Products, https://doi.org/10.5065/D61C1TXF, *Research Data Archive at the National Center for Atmospheric Research, Computational and Information Systems Laboratory*, Boulder, Colo. (Updated daily.) Accessed 22 Oct 2020.

Shchepetkin, A. F., & McWilliams, J. C. (2005). The regional oceanic modeling system (ROMS): A split-explicit, free-surface, topography-following-coordinate oceanic model. *Ocean Modelling*, *9*(4), 347–404. https://doi.org/10.1016/j.ocemod.2004.08.002

Shen, Y., Fichot, C. G., & Benner, R. (2012). Floodplain influence on dissolved organic matter composition and export from the Mississippi-Atchafalaya River system to the Gulf of Mexico. *Limnology and Oceanography*, *57*(4), 1149–116. https://doi.org/10.4319/lo.2012.57.4.1149

Skamarock, W. C., Klemp, J. B., Dudhi, J., Gill, D. O., Barker, D. M., Duda, M. G., … Powers, J. G. (2005). A Description of the Advanced Research WRF Version 3. *Technical Report*, (June), 113. https://doi.org/10.5065/D6DZ069T

Smith, S. V., & Hollibaugh, J. T. (1993). Coastal metabolism and the oceanic organic carbon balance. *Reviews of Geophysics*, *31*(1), 75–89. https://doi.org/10.1029/92RG02584

Stackpoole, S. M., Stets, E. G., Clow, D. W., Burns, D. A., Aiken, G. R., Aulenbach, B. T., … Striegl, R. G. (2017). Spatial and temporal patterns of dissolved organic matter quantity and quality in the Mississippi River Basin, 1997–2013. *Hydrological Processes*, *31*(4), 902–915. https://doi.org/10.1002/hyp.11072

Strom, S. L., & Strom, M. W. (1996). Microplankton growth, grazing, and community structure in the northern Gulf of Mexico. *Marine Ecology Progress Series*, *130*, 229–240. doi:10.3354/meps130229

Sunda, W. G., & Cai, W. J. (2012). Eutrophication induced CO2-acidification of subsurface coastal waters: Interactive effects of temperature, salinity, and atmospheric P CO2. *Environmental Science and Technology*, *46*(19), 10651–10659.

https://doi.org/10.1021/es300626f

Tao, B., Tian, H., Ren, W., Yang, J., Yang, Q., He, R., … Lohrenz, S. (2014). Increasing Mississippi river discharge throughout the 21st century influenced by changes in climate, land use, and atmospheric CO2. *Geophysical Research Letter*, *41*(14), 4978–4986. https://doi.org/10.1002/2014GL060361.Received

Todd-Brown, K. E. O., Randerson, J. T., Hopkins, F., Arora, V., Hajima, T., Jones, C., … Allison, S. D. (2014). Changes in soil organic carbon storage predicted by Earth system models during the 21st century. *Biogeosciences*, *11*(8), 2341–2356. https://doi.org/10.5194/bg-11-2341-2014

Torres, R., Pantoja, S., Harada, N., González, H. E., Daneri, G., Frangopulos, M., … Fukasawa, M. (2011). Air-sea CO2 fluxes along the coast of Chile: From CO2 outgassing in central northern upwelling waters to CO2 uptake in southern Patagonian fjords. *Journal of Geophysical Research: Oceans*, *116*(9), 1–17. https://doi.org/10.1029/2010JC006344

Turner, J. T. (2015). Zooplankton fecal pellets, marine snow, phytodetritus and the ocean's biological pump. *Progress in Oceanography*, *130*, 205–248. https://doi.org/10.1016/j.pocean.2014.08.005

Wallmann, K., Aloisi, G., Haeckel, M., Tishchenko, P., Pavlova, G., Greinert, J., ... & Eisenhauer, A. (2008). Silicate weathering in anoxic marine sediments. *Geochimica et Cosmochimica Acta*, *72*(12), 2895-2918. https://doi.org/10.1016/j.gca.2008.03.026

Wang, H., Hu, X., Cai, W. J., & Rabalais, N. N. (2016). Comparison of fCO 2 trends in river dominant and ocean dominant ocean margins. *American Geophysical Union*, AH24A-0039.

Wang, X., Cai, Y., Guo, L., & Dist, V. in abundance and size. (2013). Variations in abundance and size distribution of carbohydrates in the lower Mississippi River, Pearl River and Bay of St Louis. *Estuarine, Coastal and Shelf Science*, *126*, 61–69. https://doi.org/10.1016/j.ecss.2013.04.008

Wanninkhof, R. (1992). Relationship between wind speed and gas exchange over the ocean. *Journal of Geophysical Research: Oceans*, *97*(C5), 7373-7382. https://doi.org/10.1029/92JC00188

Wanninkhof, R. (2014). Relationship between wind speed and gas exchange over the ocean revisited. *Limnology and Oceanography: Methods*, *12*(JUN), 351–362. https://doi.org/10.4319/lom.2014.12.351

Wanninkhof, R., Zhang, J.-Z., Baringer, M. O., Langdon, C., Cai, W.-J., Salisbury, J. E., & Byrne, R. H. (2013). Partial pressure (or fugacity) of carbon dioxide, dissolved inorganic carbon, alkalinity, temperature, salinity and other variables collected from Surface underway, discrete sample and profile observations using Alkalinity titrator, Barometric pressure se. *NOAA National Centers for Environmental Information. Dataset. Https://Doi.Org/10.3334/Cdiac/Otg.Clivar_nacp_east_coast_cruise_2007.*, [Accessed 2021-05-24].

Wanninkhof, R., Zhang, J.-Z., Baringer, M. O., Langdon, C., Cai, W.-J., Salisbury, J. E., & Byrne, R. H. (2016). Partial pressure (or fugacity) of carbon dioxide, dissolved inorganic carbon, pH, alkalinity, temperature, salinity and other variables collected from discrete sample and profile observations using CTD, bottle and other instruments from NOAA Ship RONALD H. *NOAA National Centers for Environmental Information. Dataset. Https://Doi.Org/10.3334/Cdiac/Otg.Coastal_gomecc2.*, [Accessed 2021-05-24].

Wang, X., Cai, Y., & Guo, L. (2013). Variations in abundance and size distribution of carbohydrates in the lower Mississippi River, Pearl River and Bay of St Louis. *Estuarine, Coastal and Shelf Science*, *126*, 61-69. https://doi.org/10.1016/j.ecss.2013.04.008

Wanninkhof, R., Triñanes, J., Park, G. H., Gledhill, D., & Olsen, A. (2019). Large Decadal Changes in Air-Sea CO2 Fluxes in the Caribbean Sea. *Journal of Geophysical Research: Oceans*, *124*(10), 6960–6982. https://doi.org/10.1029/2019JC015366

Warner, J. C., Armstrong, B., He, R., & Zambon, J. B. (2010). Development of a Coupled Ocean-Atmosphere-Wave-Sediment Transport (COAWST) Modeling System. *Ocean Modelling*, *35*(3), 230–244. https://doi.org/10.1016/j.ocemod.2010.07.010

Wilson, R. W., Millero, F. J., Taylor, J. R., Walsh, P. J., Christensen, V., Jennings, S., & Grosell, M. (2009). Contribution of fish to the marine inorganic carbon cycle. *Science*, *323*(5912), 359–362. DOI: 10.1126/science.1157972

Wollast, R., & Mackenzie, F. T. (1989). Global biogeochemical cycles and climate. *Climate and Geo-Sciences*, *Springer,* 453–473. DOI: 10.1007/978-94-009-2446-8_26

Xu, Y. J., & DelDuco, E. M. (2017). Unravelling the relative contribution of dissolved carbon by the Red River to the Atchafalaya River. *Water*, *9*(11), 871. https://doi.org/10.3390/w9110871

Xue, Z., He, R., Fennel, K., Cai, W.-J., Lohrenz, S., Huang, W.-J., … Zang, Z. (2016). Modeling pCO 2 variability in the Gulf of Mexico. *Biogeosciences*, *13*(15), 4359–4377. https://doi.org/10.5194/bg-13-4359-2016

Yao, H., & Hu, X. (2017). Responses of carbonate system and CO2 flux to extended drought and intense flooding in a semiarid subtropical estuary. *Limnology and Oceanography*, *62*, S112–S130. https://doi.org/10.1002/lno.10646

Zang, Z., Xue, Z. G., Xu, K., Bentley, S. J., Chen, Q., D'Sa, E. J., & Ge, Q. (2019). A Two Decadal (1993–2012) Numerical Assessment of Sediment Dynamics in the Northern Gulf of Mexico. *Water*, *11*(5), 938. https://doi.org/10.3390/w11050938

Zang, Z., Xue, Z. G., Xu, K., Bentley, S. J., Chen, Q., D'Sa, E. J., Zhang, L., Ou, Y. (2020). The role of sediment-induced light attenuation on primary production during Hurricane Gustav (2008). *Biogeosciences*, *17*(20), 5043–5055. https://doi.org/10.5194/bg-17-5043-2020

Zeebe, R., & Wolf-Gladrow, D. (2001). CO2 in Seawater: Equilibrium, Kinetics, Isotopes. *Elsevier, Amsterdam*, 1–83.

Zhong, S., & Mucci, A. (1989). Calcite and aragonite precipitation from seawater solutions of various salinities: Precipitation rates and overgrowth compositions. *Chemical geology*, *78*(3-4), 283-299. https://doi.org/10.1016/0009-2541(89)90064-8

Zondervan, I., Zeebe, R. E., Rost, B., & Riebesell, U. (2001). Decreasing marine biogenic calcification: A negative feedback on rising atmospheric pCO2. *Global Biogeochemical Cycles*, *15*(2), 507–516. https://doi.org/10.1029/2000GB001321

Zuddas, P., & Mucci, A. (1998). Kinetics of calcite precipitation from seawater: II. The influence of the ionic strength. *Geochimica et Cosmochimica Acta*, *62*(5), 757-766. https://doi.org/10.1016/S0016-7037(98)00026-X